NAVORD REPORT 1488 (VOL. 3)

HANDBOOK OF SUPERSONIC AERODYNAMICS

SECTION 7

THREE-DIMENSIONAL AIRFOILS

A BUREAU OF ORDNANCE PUBLICATION

NAVORD REPORT 1488 (VOL. 3)

HANDBOOK OF SUPERSONIC AERODYNAMICS

SECTION 7

THREE-DIMENSIONAL AIRFOILS

PRODUCED AND EDITED BY THE AERODYNAMICS HANDBOOK STAFF OF THE JOHNS HOPKINS UNIVERSITY APPLIED PHYSICS LABORATORY, SILVER SPRING, MARYLAND UNDER CONTRACT NORD 7386 WITH THE BUREAU OF ORDNANCE, DEPARTMENT OF THE NAVY. THE TEXT OF THIS SECTION WAS PREPARED LARGELY BY R. M. PINKERTON. THE SELECTION AND TECHNICAL REVIEW OF THIS MATERIAL WERE FUNCTIONS OF A REVIEWING COMMITTEE OF THE LABORATORY CONSISTING OF IONE D. V. FARO, LESTER L. CRONVICH, AND ROBERT N. SCHWARTZ (CHAIRMAN).

For sale by the Superintendent of Documents, U. S. Government Printing Office
Washington 25, D. C. - Price $1.50

AUGUST 1957

Series Contents

HANDBOOK OF SUPERSONIC AERODYNAMICS

Volume 3 - Section 7

Preface

A preface to the entire Handbook of Supersonic Aerodynamics appears in Volume 1 and includes a brief history of the project. As stated in Volume 1, "The primary criterion used in selecting material for the Handbook is its expected usefulness to designers of supersonic vehicles. Thus a collection of data directly useful in the design of supersonic vehicles, results of the more significant experiments, and outlines of basic theory are included ...."

The present edition of the Handbook, printed and distributed by the Bureau of Ordnance, is being published in separate sections as material becomes available. The contents of the entire work is given on the back of the title page. It may be noted, the majority of sections of the Handbook are being prepared by individual authors for the Applied Physics Laboratory. Those sections are noted for which an early publication date is expected. The selection of material, editing, and technical review of the Handbook of Supersonic Aerodynamics continue to be carried out by an editor and a technical reviewing committee at the Applied Physics Laboratory.

Volume 3 of the Handbook of Supersonic Aerodynamics contains three closely related sections, "Two-Dimensional Airfoils" (Section 6), "Three-Dimensional Airfoils" (Section 7), and "Bodies of Revolution" (Section 8). A fourth related section on wing-body interference (Section 9) is placed in Volume 4 with sections on stability and control because of its importance to this later subject.

The staff of the Aerodynamics Handbook Project at the Applied Physics Laboratory gives grateful acknowledgment to the Aeromechanics Division of the Defense Research Laboratory of The University of Texas for the large amount of computational work carried out by them for the Sections 6 and 7 of the Handbook.

The numbering system of Volume 3 is essentially the same as that used in the last preceding volumes.

Agencies and individuals interested in the aeronautical sciences are invited to submit and to recommend material for inclusion in the Handbook; full credit will be given for all such material used. Regarding the selection of material and the preparation of the volumes in the Handbook Series, the Applied Physics Laboratory earnestly solicits constructive criticisms and suggestions. Correspondence relating to the editing of the Handbook should be directed to

Editor and Supervisor, Aerodynamics Handbook Project
Applied Physics Laboratory
The Johns Hopkins University
8621 Georgia Avenue
Silver Spring, Maryland

Communications concerning distribution of the Handbook should be directed to

Chief, Bureau of Ordnance
Department of the Navy
Washington 25, D. C.

SECTION 7 - THREE-DIMENSIONAL AIRFOILS

CONTENTS

FIGURES

*Figures are numbered so as to correspond to the subsection in which they are discussed.

SECTION 7 - THREE-DIMENSIONAL AIRFOILS

Primary Symbols

a	velocity of sound
A	aspect ratio: $\frac{b^2}{S}$
b	wing span (twice the distance from the tip to the root chord): 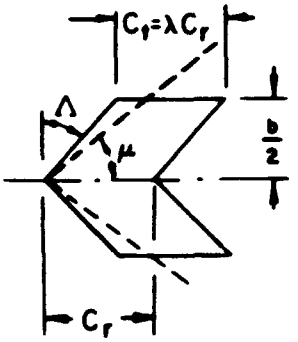
c	wing chord
C_D	drag coefficient: $\frac{\text{Drag Force}}{\frac{1}{2}\rho V^2 S}$
C_L	lift coefficient: $\frac{\text{Lift Force}}{\frac{1}{2}\rho V^2 S}$
C_{L_α}	lift-curve slope: $\frac{dC_L}{d\alpha}$
C_m	pitching moment coefficient: $C_m = \frac{\text{pitching moment about the apex of the leading edge}}{\frac{1}{2}\rho V^2 S c_r}$ (where a positive moment is defined as a moment tending to tilt leading edge upward)
C_{m_α}	moment-curve slope: $\frac{dC_m}{d\alpha}$
c_p	pressure coefficient: $\frac{p - p_\infty}{\frac{1}{2}\rho V^2}$

$E\left(\sqrt{1 - (\beta \cot \Lambda)^2}\right)$	complete elliptical integral of the second kind, of modulus $\sqrt{1 - (\beta \cot \Lambda)^2}$
g	source intensity per unit area
M	Mach number: $\frac{V}{a}$
p	pressure
S	wing planform area (two panels)
t	thickness of wing profile
$\frac{t}{c}$	thickness ratio
u, v, w	components of perturbation velocity in x-, y-, z- directions
V	velocity of the undisturbed stream
x, y, z	rectangular coordinates
x_{cp}	moment arm of wing elemental lifting area
α	angle of attack
β	$\sqrt{M^2 - 1}$
δ	tip rake angle (angle which tip makes with the root chord direction; defined as positive when the tip is raked inboard)
Λ	leading edge sweepback (angle which the leading edge makes with normal to root chord direction)
Λ_T	trailing edge sweepback (angle which the trailing edge makes with normal to root chord direction)
λ	taper ratio (tip chord divided by root chord for unraked wings with straight leading and trailing edges)
μ	Mach angle: $\sin^{-1} \frac{1}{M}$

ξ , η, ζ	rectangular coordinates used to specify source distributions
ρ	density (of ambient fluid)
ϕ	perturbation velocity potential
Φ	total velocity potential
ω_x	slope of wing surface measured with respect to the x-direction

Auxiliary Symbols

Subscripts

l	reference to lower surface of wing
r	reference to root section of wing
t	reference to tip section of wing
u	reference to upper surface of wing
x, y, z	partial derivatives with respect to coordinate variables, e.g., $\phi_x = \frac{\partial \phi}{\partial x}$
∞	reference to the undisturbed stream conditions

SECTION 7 - THREE-DIMENSIONAL AIRFOILS

This section of the Handbook of Supersonic Aerodynamics was prepared at the Applied Physics Laboratory of The Johns Hopkins University. Many of the formulae and graphs for lift and moment characteristics of three-dimensional airfoils were especially prepared for this section by the Defense Research Laboratory of The University of Texas.

700 Introduction

This section of the Handbook presents the aerodynamic characteristics of a limited class of finite wings in a convenient form for use in design calculations. The treatment of finite wings is severely limited to uncambered wings with zero angle of attack for which thickness ratio and position of maximum thickness are held at a constant value. Section 6 of the Handbook (Two-Dimensional Airfoils) may be used for guidance in estimating viscosity effects and the effect of changing the angle of attack, thickness ratio, camber, and position of maximum thickness.

Section 7 treats wings alone and ignores the fact that, in practical application, wings are attached to bodies. Bodies alone are discussed in Section 8 of the Handbook (Bodies of Revolution), and interference effects of the wing-body combination are treated in detail in Section 9 of the Handbook (Mutual Interference Phenomena).

Section 7 also includes a summary of the underlying theory with particular emphasis on the limiting conditions which affect the range of applicability of the data presented.

700.1 Scope of Contents

Theoretical airfoil characteristics for lift, pitching moment, and pressure drag are computed by the method of supersonic source distributions. They are presented in graphical form using non-dimensional parameters which define the aerodynamic and geometric properties of wings in supersonic flow. The lift and moment analysis is discussed first because much of it is also a basic consideration in the drag analysis. The calculations at zero angle of attack involve linearized theory only. The reader is referred to Section 6 of the Handbook (Two-Dimensional Airfoils) for a comparison of linearized theory and higher order theories.

Throughout the discussion theoretical analyses are reduced to a minimum consistent with intelligent use of the data, and a reference is made to the original sources containing the more detailed analyses. Sample calculations are included to demonstrate the practical use of the graphs in determining the aerodynamic characteristics of several wing configurations at specified flight conditions.

A brief comparison of theory and experiment is included in order to provide a convenient basis for estimating the accuracy and reliability of theoretical predictions from the linearized theory.

701 Resume of Basic Theory

A resume of basic theory is sketched out here to assist the reader in his understanding and interpretation of the material presented in graphical form. This discussion is limited to a consideration of a supersonic source solution. The more complex questions, e.g., boundary conditions, conical flow solutions, and so forth, are referenced where appropriate.

701.1 Basic Flow Assumptions

The subsequent analysis is based on the assumption of a fluid prescribed by the following characteristics:

a. Compressible fluid
b. Inviscid fluid, without heat transfer
c. Absence of all external force fields
d. Steady motion, i.e., flow quantities are independent of time
e. Irrotational flow, i.e., the flow field is free of vorticity (see item g below)
f. Shock waves are infinitely weak
g. Adiabatic processes, i.e., no heat transfer at the boundaries

701.2 General Equation of Motion

The equation of motion governing the flow under these conditions is expressed in the total velocity potential form (Ref. 1, p. 2.17, Eq. 2.31) as follows:

$$\left[1 - \frac{\Phi_x^2}{a^2}\right]\Phi_{xx} + \left[1 - \frac{\Phi_y^2}{a^2}\right]\Phi_{yy} + \left[1 - \frac{\Phi_z^2}{a^2}\right]\Phi_{zz} - 2\Phi_{yz}\frac{\Phi_y \Phi_z}{a^2} - 2\Phi_{zx}\frac{\Phi_z \Phi_x}{a^2} - 2\Phi_{xy}\frac{\Phi_x \Phi_y}{a^2} = 0 , \qquad (701.2\text{-}1)$$

where Φ is the total velocity potential defined by

$$u' = \Phi_x ,$$

$$v' = \Phi_y ,$$

$$w' = \Phi_z ,$$

and

$$\Phi_x = \frac{\partial \Phi}{\partial x} , \text{ etc.}$$

The primed symbols represent the total velocity components as contrasted with perturbation velocities which are designated by symbols without primes.

Here $a = \sqrt{\left(\frac{\partial p}{\partial \rho}\right)}$ is the velocity of propagation of an infinitesimal pressure wave at constant entropy (sonic velocity).

701.21 Linearized Equation of Motion

Solutions for this second order non-linear differential equation (Eq. 701.2-1) have been found for only a limited number of cases and, therefore, some simplification is necessary if any practical applications are to be made. In applications to the flow past finite wings, a large range of important wing configurations meet the requirements of the linearization of this equation. This linearization is a consequence of using the small perturbation theory in which it is assumed that the disturbances produced by a body in a fluid are very small compared to the velocity of the undisturbed flow. The wings of aircraft flying at supersonic speeds are usually sufficiently thin so that, at small angles of attack, the velocity disturbances can be assumed to satisfy the requirements of the small perturbation theory at all points in the flow, except in the immediate vicinity of the subsonic leading edge.

The linearization of Eq. 701.2-1 by the theory of small perturbations is accomplished as follows:

a. The total velocity components u', v', w' in the undisturbed stream are:

$$u' = V \text{ (constant)}$$
$$v' = 0$$
$$w' = 0$$

b. The corresponding total velocity components in the presence of the disturbance are:

$$u' = V + u$$
$$v' = v$$
$$w' = w$$

where u, v, and w, the disturbance velocities, are limited by the small perturbation theory to

$$u \ll V, \quad v \ll V, \quad w \ll V.$$

Since the flow external to the disturbing body is assumed irrotational, a perturbation velocity potential, ϕ, is introduced defined by

$$u = \phi_x, \quad v = \phi_y, \quad w = \phi_z.$$

Substituting in the general potential Eq. 701.2-1, and neglecting terms of second order and higher in the perturbation velocities and their first derivatives, we arrive at the following linearized form of the equation of motion:

$$\left[M_\infty^2 - 1\right] \phi_{xx} - \phi_{yy} - \phi_{zz} = 0 , \qquad (701.21\text{-}1)$$

where $M_\infty \equiv \frac{V}{a_\infty}$ is the Mach number of the undisturbed flow. This linearization leads to solutions of the same degree of accuracy as that given by the first order theory for two-dimensional airfoils which was treated in Section 6 of the Handbook.

701.3 Solution of Linearized Equation by the Method of Sonic Source Distributions

An elementary solution of the linearized form of the equation of motion (Eq. 701.21-1) is defined by the following function (see Puckett, Ref. 2, Eq. 3):

$$\phi(x, y, z) = \frac{-C}{\sqrt{(x-\xi)^2 - \beta^2\left[(y-\eta)^2 + (z-\zeta)^2\right]}} , \qquad (701.3\text{-}1)$$

where $$\beta^2 = M_\infty^2 - 1 .$$

The function defined by Eq. 701.3-1 represents the potential at the point (x, y, z) due to a point source of strength proportional to C and located at the point P (ξ, η, ζ) (see Heaslet and Lomax, Ref. 3, p. 149). This function becomes imaginary outside the cone shown in the figure on the next page and described by the equation,

$$(x-\xi)^2 - \beta^2\left[(y-\eta)^2 + (z-\zeta)^2\right] = 0. \qquad (701.3\text{-}2)$$

This cone has its vertex at the point P (ξ, η, ζ) and has a semi-vertex angle of

$$\mu = \tan^{-1}\frac{1}{\beta} = \sin^{-1}\frac{1}{M} .$$

It corresponds to the Mach cone formed by the stationary wave front produced in a flow at Mach number M_∞ by a disturbance at P (ξ, η, ζ).

489030 O - 59 - 2

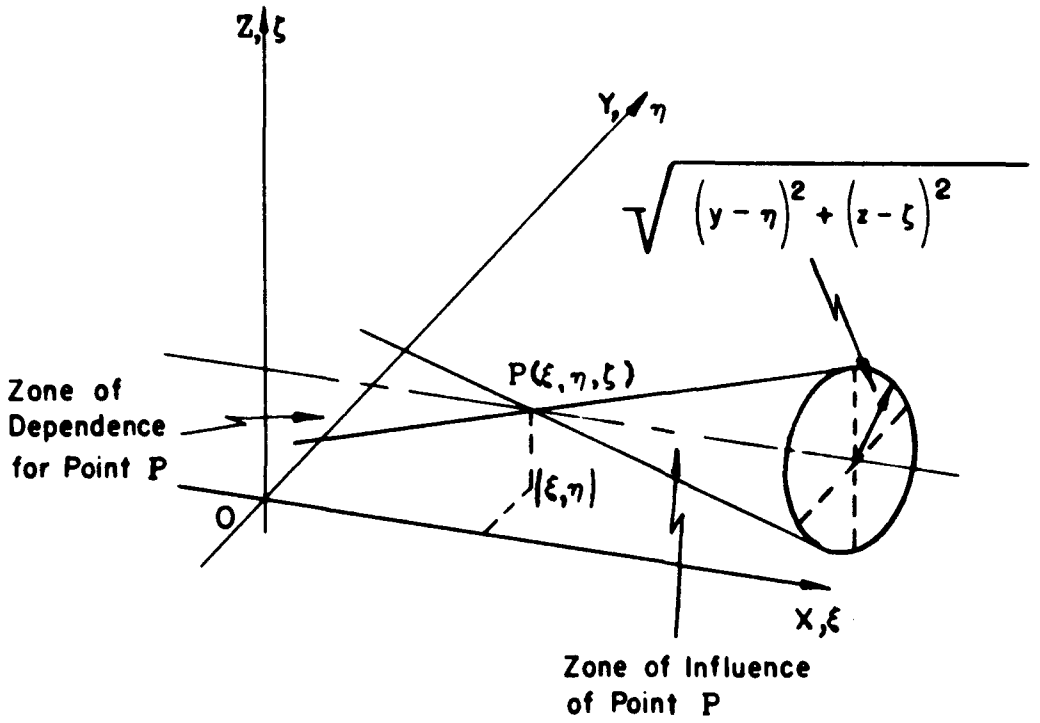

A disturbance at P (ξ , η, ζ) cannot be felt outside the cone downstream from this point, but is felt within the cone, thereby defining zones of inaction and action respectively. The zone of action is noted as the Zone of Influence in the figure above. Likewise, conditions at P (ξ , η, ζ) depend only on events occurring within the cone upstream of the point. This zone is known as the Zone of Dependence.

Solutions of more general applicability are obtained by assuming distributions of sources of varying strength. This is permissible since the differential equation is linear and the principle of superposition applies. Puckett (Ref. 2) has applied the distributed source solution to the evaluation of the flow over a thin triangular planform wing. The analysis is summarized here as a means of illustrating the application of the small perturbation theory to the determination of wing characteristics at supersonic speeds. The thin wings under consideration are assumed to lie essentially in the xy-plane and the sources are distributed in that plane. Letting g represent the source strength per unit area, the differential element of the perturbation velocity potential, $d\phi$, is obtained by writing (g $d\xi$ $d\eta$) in place of C in Eq. 701.3-1. Therefore,

$$d\phi = \frac{-g \, d\xi \, d\eta}{\sqrt{(x-\xi)^2 - \beta^2 \left[(y-\eta)^2 + z^2 \right]}}, \qquad (701.3\text{-}3)$$

where $g = g(\xi, \eta)$.

701.31 Determination of Velocity Potential for Thin Wings

The velocity potential at any point on the wing surface is obtained by the integration of Eq. 701.3-3 over the wing area inclosed within the Zone of Influence for that point. Puckett (Ref. 2) demonstrated that the source intensity, g, at any point is dependent only upon local conditions, and is given by

$$g = \frac{w}{\pi} . \qquad (701.31\text{-}1)$$

The boundary condition simply requires that the local velocity be parallel to the wing surface at any point, that is,

$$\omega_x = \frac{w}{V} , \qquad (701.31\text{-}2)$$

where ω_x is the slope of the wing surface relative to the x-direction at a given point. Since these wings are assumed to lie in the xy-plane, it is sufficient to satisfy the boundary condition in that plane ($z = 0$). The velocity potential at the point (x, y) becomes, after substitution from Eqs. 701.31-1 and 701.31-2 in Eq. 701.3-3,

$$\phi(x, y) = -\frac{V}{\pi} \iint_{\Delta S} \frac{\omega_x \, d\xi \, d\eta}{\sqrt{(x - \xi)^2 - \beta^2 (y - \eta)^2}} , \qquad (701.31\text{-}3)$$

where ΔS is the area of source distribution intercepted by the forecone from the point (x, y) and thus lies within the Zone of Influence.

701.32 Perturbation Velocity and Pressure Coefficient

The horizontal perturbation velocity in the x-direction, ϕ_x, is obtained from Eq. 701.31-3. The pressure coefficient, defined as

$$c_p = \frac{p - p_\infty}{\frac{1}{2}\rho V^2} , \qquad (701.32\text{-}1)$$

is

$$c_p = \frac{-2u}{V} , \qquad (701.32\text{-}2)$$

as obtained from the linearized theory.

701.4 Infinite Triangular Wing

The infinite triangular wing is used as a basic configuration in supersonic flow analysis somewhat analogously to the infinite aspect ratio wing in subsonic flow analysis. The properties of finite wings in supersonic flow are frequently obtained by the superposition of triangular wing components.

701.41 Supersonic and Subsonic Leading Edges

In supersonic wing theory the treatment of supersonic flow over wing surfaces is divided into two main divisions. These divisions are referred to as the supersonic and subsonic leading edge conditions in which the velocity component normal to the leading edge is supersonic and subsonic respectively. These conditions are also identified by the position of the leading edge with respect to the Mach line from a point on the leading edge (as shown in the figure below).

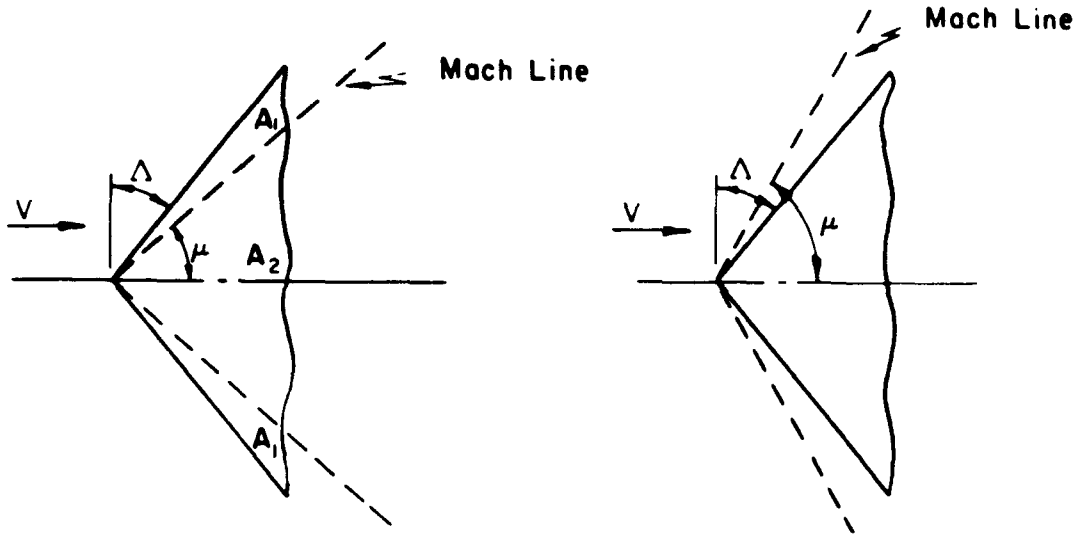

$\mu < (\frac{\pi}{2} - \Lambda)$ or $\beta \cot \Lambda > 1$

(a) Supersonic Leading Edge

$\mu > (\frac{\pi}{2} - \Lambda)$ or $\beta \cot \Lambda < 1$

(b) Subsonic Leading Edge

With supersonic leading edges, pressure changes due to disturbances on one surface cannot be transmitted forward and thence around the leading edge to modify the flow over the other surface. The flow over upper and lower surfaces, therefore, can be treated independently. On the other hand, a subsonic leading edge condition permits the transmission of pressure disturbances from one surface to the other and these interferences must be taken into consideration in the analysis of the flow over the wing surfaces.

701.42 Horizontal Perturbation Velocity for a Triangular Wing

Puckett's analysis (Ref. 2) treats the infinite triangular wing with a supersonic leading edge. The Mach line from the wing apex in this instance divides the wing surface into two regions, and the integration (indicated by Eq. 701.31-3) is accomplished separately for each of these regions. The horizontal perturbation velocity, u, is constant in the region ahead of the Mach line (Region A_1, Fig. (a) on the preceding page), and is given by the following equation (Puckett, Ref. 2, Eq. 34):

$$\frac{u}{V} = \frac{-\omega_x \, (\beta \cot \Lambda)}{\beta \sqrt{(\beta \cot \Lambda)^2 - 1}} , \qquad (701.42\text{-}1)$$

In the region behind the Mach line (Region A_2, Fig. (a)) the perturbation velocity is given by the equation (Ref. 2, Eq. 35):

$$\frac{u}{V} = \frac{-2\omega_x \, (\beta \cot \Lambda)}{\pi \beta \sqrt{(\beta \cot \Lambda)^2 - 1}} \cos^{-1} \sqrt{\frac{1 - \beta^2 (\frac{y}{x})^2}{(\beta \cot \Lambda)^2 - \beta^2 (\frac{y}{x})^2}} . \qquad (701.42\text{-}2)$$

Stewart, using the method of conformal transformation, determined the flow characteristics for an infinite triangular wing with subsonic leading edge and his results (Ref. 5, Eq. 45), rewritten in the present notation, give

$$\frac{u}{V} = \frac{-\omega_x \, (\beta \cot \Lambda)^2}{\beta \sqrt{(\beta \cot \Lambda)^2 - \beta^2 (\frac{y}{x})^2}} \cdot \frac{1}{E\left(\sqrt{1 - (\beta \cot \Lambda)^2}\right)} , \qquad (701.42\text{-}3)$$

where $E\left(\sqrt{1 - (\beta \cot \Lambda)^2}\right)$ is the complete elliptic integral of the second kind, of modulus $\sqrt{1 - (\beta \cot \Lambda)^2}$. Equations 701.42-2 and 701.42-3 show that the perturbation velocity, u, and hence the pressure coefficient, $c_p = \frac{-2u}{V}$, remain constant along radial lines drawn from the apex, which, according to Busemann (Ref. 6), is characteristic of conical flow phenomena.

701.5 Analysis of Finite Wing Planforms

The aerodynamic characteristics of thin, flat, sweptback finite wings are determined by suitable modification and application of the results for infinite flat triangular wings. When the boundary of a finite configuration crosses the basic triangular wing, a correction must be determined which in effect cancels the pressure field of the infinite triangular wing beyond the boundary of the finite configuration without altering the specified boundary conditions. In some instances, e.g., for a triangular planform, it is sufficient to locate the trailing edge boundary and disregard the downstream portion of the pressure field of the wing, since pressure disturbances cannot be transmitted upstream. An example of this type of analysis is given in the computation of the drag of a triangular planform with a double wedge cross section (see Subsection 702.22).

Other planforms having supersonic trailing edges require more elaborate and detailed pressure-field cancelling techniques to account for the effect of disturbances radiating from planform discontinuities such as the leading edge of a tip chord. The flow about wings moving at supersonic speeds with subsonic trailing edges must satisfy the well-known Kutta condition which requires the velocity to be finite at the trailing edge.

The analysis and data presented herein are limited to wings having sweptback leading edges only. Data for wings with sweptforward leading edges can be determined by means of the reversibility theorem, discussed later (see Subsection 702.3), from data for equivalent wings having sweptback leading edges.

The source distribution methods cited in Puckett (Ref. 2) and Evvard (Ref. 7) offer the most convenient means of calculating the aerodynamic characteristics for planforms with supersonic leading and trailing edges. The calculation of the flow properties for wings with subsonic leading edges is accomplished through the use of solutions presented in Stewart (Ref. 5) and Lagerstrom (Ref. 8) for the infinite triangular wing plus suitable pressure cancelling techniques. Two such methods or techniques appear to be generally used. One of these methods, discussed by Mirels (Ref. 9), uses supersonic doublets and is applicable to curved boundaries. The second method, discussed by Cohen (Ref. 10), uses the superposition of conical flow fields originally introduced by Busemann (Ref. 6)*. The details of these pressure-field cancellation techniques are, however, beyond the scope of this Handbook.

---

*An extensive table of conical flow functions is given in the Princeton Series, Vol. VII, pp. 156-165 (Ref. 37).

702 Calculation of Wing Characteristics

The lift, moment, and drag curves of representative wing planforms are presented in this section of the Handbook. These results are based on the method of supersonic source distributions treated in Subsections 701 through 701.31 above. When the wing is taken at an angle of attack, the flow must satisfy the Kutta condition (i.e., finite velocity at the trailing edge). A trailing edge for which the normal component of flow is supersonic automatically satisfies this condition. General solutions for the subsonic trailing edge condition have not been obtained. Consequently, the lift and moment data presented in this section are restricted to supersonic trailing edges. The drag results do not experience this limitation because they are restricted here to zero angle of attack.

702.1 Lift and Moment Characteristics

The limitations of the small perturbation linearized theory for supersonic flow restricts the applications to thin wings at small angles of attack. The slopes of the lift and moment curves with angle of attack depend on the wing planform only and not on the camber and thickness. The wing, therefore, can be treated as a flat plate, and lift (under the small angle of attack limitation) is assumed equal to the normal pressure force obtained by the integration of the pressure over the surface of the wing. Therefore, the lift is given by

$$L = \int_S (p_l - p_u)\,dS ,$$

where the subscripts l and u refer to the lower and upper surfaces respectively and S is the wing planform area. This expression for the lift is rewritten by use of Eqs. 701.32-1 and 701.32-2 to obtain a lift coefficient expressed in terms of the perturbation velocity, u:

$$C_L \equiv \frac{L}{\frac{1}{2}\rho V^2 S} ,$$

$$= \frac{2}{S} \int_S \left(\frac{u_u}{V} - \frac{u_l}{V} \right) dS.$$

The ratio of the perturbation velocity to the free stream velocity, $\frac{u}{V}$, is shown by Eqs. 701.42-1, 701.42-2, and 701.42-3 to be proportional to the slope of the wing surface, ω_x. The upper and lower surfaces of a flat plate wing are parallel and, under the small angle of attack

limitation, the slopes are equal to $(-\alpha)$ and (α) respectively, where α is the angle of attack in radians. Therefore, the slope of the lift curve is given by

$$C_{L_\alpha} \equiv \frac{dC_L}{d\alpha} ,$$

$$= \frac{4}{S} \int_S \frac{u}{V\alpha} \, dS. \qquad (702.1\text{-}1)$$

The integral expression for the wing pitching-moment-curve slope is

$$C_{m_\alpha} \equiv \frac{dC_m}{d\alpha} ,$$

$$= \frac{4}{S} \int_S \frac{u}{V\alpha} \left[\frac{x_{cp}}{c_r}\right] dS , \qquad (702.1\text{-}2)$$

where x_{cp} is the distance from the center of the element of area to the moment axis, and c_r is the wing chord at its root section.

The evaluations of Eqs. 702.1-1 and 702.1-2 are accomplished most conveniently by use of the superposition principle, since the perturbation velocity, u, is not known as a single function of the wing surface coordinates. The triangular wing is used as a basic configuration for which basic lift and moment-curve slopes are obtained by the use of Eqs. 701.42-1 and 701.42-2, or 701.42-3 in Eqs. 702.1-1 and 702.1-2 depending upon whether the leading edge is supersonic or subsonic. The integrations are simplified by using a triangular element of area with its apex at the wing apex and bounded by radial lines and a segment of the wing boundary. This reduces the double integrals in Eqs. 702.1-1 and 702.1-2 to single integrals, since the function for $\frac{u}{V\alpha}$ remains constant along a radial line. The new variable is $\frac{\beta y}{x}$, as used by Cohen (Ref. 10).

The methods described in the preceding paragraphs have been applied by various researchers to the determination of the lift and moment-curve slopes for commonly used finite wings moving at supersonic speeds. Formulas resulting from these analyses are presented in Cohen (Ref. 10) and Piland (Ref. 11) along with references to the original sources. Additional applications have been made at the Defense Research Laboratory of The University of Texas (Ref. 12). This latter reference, which also includes charts presenting the lift and moment-curve data from all of the above sources, is used as the main source of the numerical data presented in this section of the Handbook.

702.11 Parameters for Lift and Moment Data

A review of the existing data and of the methods of presentation has led to the choice of the following parameters for the presentation of the lift and moment data:

βA	Mach number-aspect ratio parameter
$\beta \cot \Lambda$	Mach number-leading edge sweepback parameter
βC_{L_α}	Mach number-lift-curve slope parameter
βC_{m_α}	Mach number-moment-curve slope parameter

The variations of the Mach number-planform parameters βA and $\beta \cot \Lambda$ with Mach number for certain constant values of A and Λ are shown in Fig. 702.11-1. The planforms of swept wings with unraked tips can usually be specified by three parameters: (1) aspect ratio, A, (2) leading edge sweepback angle, Λ, and (3) taper ratio, λ. Commonly used wing planform categories are defined by the following relations.

$$A \gtreqless 4 \frac{1 - \lambda}{1 + \lambda} \cot \Lambda \quad , \qquad (702.11\text{-}1)$$

where $>$, $=$, and $<$ specify sweptback, unswept, and sweptforward trailing edges respectively. Planforms having fore and aft symmetry are defined by the relation

$$A = 2 \frac{1 - \lambda}{1 + \lambda} \cot \Lambda \qquad (702.11\text{-}2)$$

Illustrations of typical configurations so defined by this relation are shown in Fig. 702.11-1 for taper ratios of $\lambda = 0$ and $\lambda = 0.5$.

It has been shown earlier (see figure given in Subsection 701.41) that regions of subsonic and supersonic leading edges are defined by

$$\beta \cot \Lambda \lessgtr 1 \quad , \qquad (702.11\text{-}3)$$

where $<$, $=$, and $>$ specify subsonic, sonic, and supersonic leading edge respectively. Regions of subsonic and supersonic trailing edges can be defined by simple relations between the planform parameters as given on the following page.

Sweptback trailing edge:

$$\beta \cot \Lambda \gtreqless \frac{\beta A}{4\,\frac{1-\lambda}{1+\lambda} + \beta A}, \text{ or } \frac{4\,\frac{1-\lambda}{1+\lambda}\,\beta\cot\Lambda}{1-\beta\cot\Lambda} \gtreqless \beta A,$$

(702.11-4)

where the signs < , =, and > designate subsonic, sonic, and supersonic trailing edge conditions respectively.

Sweptforward trailing edge:

$$\frac{\beta A}{4\,\frac{1-\lambda}{1+\lambda} - \beta A} \gtreqless \beta\cot\Lambda, \text{ or } \beta A \gtreqless \frac{4\,\frac{1-\lambda}{1+\lambda}\,\beta\cot\Lambda}{1+\beta\cot\Lambda},$$

(702.11-5)

where < , =, and > specify subsonic, sonic, and supersonic trailing edge conditions respectively. Subsonic and supersonic trailing edge conditions are shown in the following figure.

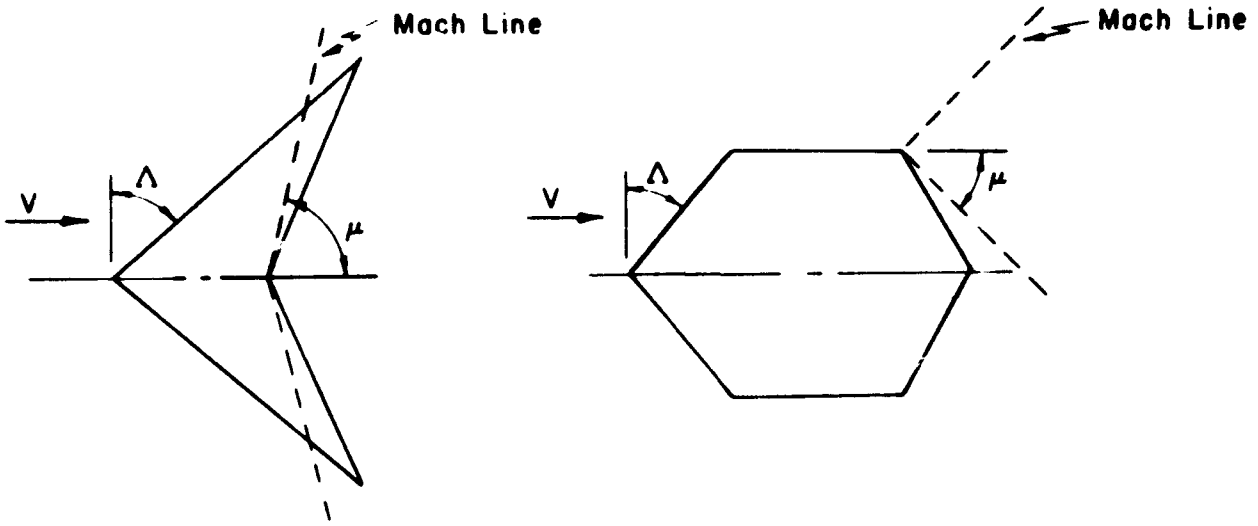

(a) Subsonic, Sweptback Trailing Edge, $\lambda = 0$

(b) Supersonic, Sweptforward Trailing Edge, $\lambda = 0.5$

Wing planforms with taper ratios, $\lambda = 0$, 0.5, and 1.0 corresponding to various combinations of βA and $\beta \cot \Lambda$ at an arbitrary Mach number of $M = 2.24$ ($\beta = 2$) are shown in Figs. 702.11-2, 702.11-3, and 702.11-4 respectively in order to illustrate the variations in planforms associated with changes in the planform parameters. The short-dashed lines shown on each diagram indicate the Mach lines for the Mach number, $M = 2.24$, given above. The apex of each wing leading edge designates the βA and $\beta \cot \Lambda$ coordinates associated with that wing planform. Equations 702.11-1 and 702.11-2 show that the unswept trailing edge and symmetrical planforms are associated with values of βA and $\beta \cot \Lambda$ lying along a radial line defined by constant values of the ratio, $\frac{\beta A}{\beta \cot \Lambda}$. The sonic leading edge and trailing edge boundaries defined by Eqs. 702.11-3, 702.11-4, and 702.11-5 are represented by solid lines shown on Figs. 702.11-2, 702.11-3, and 702.11-4. A similar figure for trapezoidal wings, for which the planform parameters are βA and $\beta \tan \delta$ is shown in Fig. 702.11-5.

702.2 Drag Characteristics

The drag of finite wings is comprised of three parts: namely, drag due to thickness of the airfoil section (usually referred to as pressure drag or wave drag at zero lift), drag due to lift* (or induced drag), and skin friction drag.

702.21 Discussion of Drag Components

The pressure drag is the integral, taken over the wing surfaces, of the drag component of the pressure acting on those surfaces. This drag is known to be zero for a body moving at subsonic speeds in a nonviscous incompressible fluid. In an actual fluid, however, there exists a wake due to the viscous boundary layer and, due to the presence of this wake, the full pressure recovery over the after portion of the wing surface is not realized. Thus, in an actual fluid, some pressure drag is always present. Nevertheless, efficient wings moving at subsonic speeds produce such very small wakes that the actual pressure drag is small and therefore is included with the experimentally-determined skin friction drag to make up the well-known profile drag of wings at subsonic speeds.

The integrated pressure drag for finite wings moving at supersonic speeds in a nonviscous compressible fluid, however, is not zero. This component of the drag is commonly referred to as the pressure drag (or wave drag) at supersonic speeds and is treated separately from skin friction drag. Pressure drag at zero lift is presented in this section of the Handbook.

---

*The drag due to lift is generally referred to as induced drag. Induced drag is made up of two parts in supersonic flow. One part is the loss of momentum in the general flow direction caused by the deflection of the airstream, i.e., the reaction to the lift force on the wing. This component of the drag in supersonic flow corresponds

(continued on following page)

The skin friction drag is the direct effect of the viscous fluid moving in a direction relative to the wing and is present at all speeds. This component of wing drag is best determined experimentally. In the absence of reliable data of this kind, however, a useful estimation of skin friction drag can be obtained by a method presented in Section 6 (Subsection 605.1) of the Handbook.

702.22 Pressure Drag at Zero Lift

The pressure drag at zero lift for a wing with a symmetrical airfoil section is given by

$$D = 2 \int_{S'} \Delta p \sin\left(\tan^{-1} \omega_x\right) dS' = 2 \int_{S} \omega_x \, \Delta p \, dS \, , \qquad (702.22\text{-}1)$$

where

ω_x is the slope of the wing surface ,

Δp is the surface pressure measured with respect to the pressure of the undisturbed stream ,

S' is the wetted area of upper (or lower) surface of the wing, and

S is the wing planform area.

Expressed as a drag coefficient, and using Eqs. 701.32-1 and 701.32-2, the above expression (Eq. 702.22-1) for zero lift drag becomes

$$C_D \equiv \frac{D}{\frac{1}{2}\rho V^2 S} = \frac{4}{S} \int_{S} \left(\frac{-u}{V\omega_x}\right) \omega_x^{\,2} \, dS \, . \qquad (702.22\text{-}2)$$

The terms within the parenthesis are grouped for the convenient application of Eqs. 701.42-1, 701.42-2, and 701.42-3, and the $\omega_x^{\,2}$ indicates the independence of the drag on the sign of the slope of the wing surface.

(continued)

to the well-known induced drag of subsonic flow. The second part is the increase in pressure drag over the pressure drag (wave drag) corresponding to zero lift. The first part of supersonic induced drag is sometimes called the induced vortex drag, while the second part is referred to as the induced wave drag.

The expressions for C_D, with $\frac{u}{V}$ given by Eqs. 701.42-1, 701.42-2, and 701.42-3, may be integrated immediately to yield the drag of a wedge shaped triangular wing with an unswept, blunt trailing edge (see Puckett, Ref. 2). However, by the principle of superposition of elementary solutions given by the linearized theory, the results given above may be extended to treat the double wedge sections discussed in Subsection 702.23. For example, the drag due to the wing segment $\overline{atmt'}$ of the inset figure can be found by superimposing the solutions for the triangular wing $\overline{att'}$ of slope ω_x and the triangular wing mtt' with slope $-\omega_x$. The drag due to a single wing segment atmt' (denoted hereafter with the subscript am) is given as a function of A_{am} and Λ_{am} of the segment in a convenient set of charts in Multhopp and Winter (Ref. 36) and reproduced in Fig. 702.22-1 of this Handbook by courtesy of the Controller, Her Brittanic Majesty's Stationery Office, England. By suitably combining solutions, the complete double wedge can be constructed. If the functions ΔF_{am}, ΔF_{mr}, and ΔF_{ar} correspond to solutions for the appropriate segments, the total drag is given by

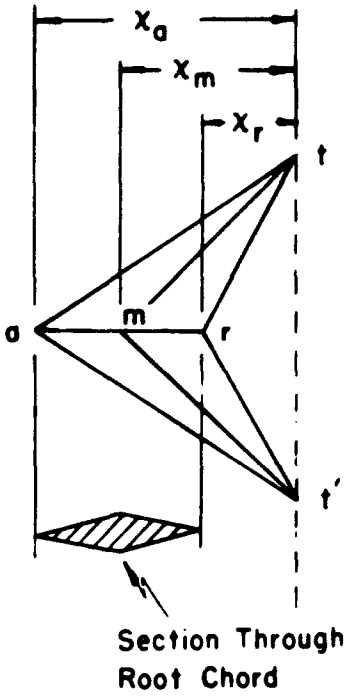

$$\frac{\beta C_D}{\left(\frac{t}{c}\right)^2} = \frac{(X_a - X_r)^2}{(X_a - X_m)(X_m - X_r)} \left(\Delta F_{am} + \Delta F_{mr} - \Delta F_{ar} \right).$$

These results are easily generalized to any polygonal cross section.

The results of Puckett for the triangular planform with an unswept trailing edge was first extended by Puckett and Stewart (Ref. 13) to wings with sweptback and sweptforward trailing edges. Similar source solutions using a somewhat different approach were found by Jones (Ref. 14). Margolis (Refs. 15, 16, and 17) applied the method of Jones (Ref. 14) to the evaluation of zero lift wave drag of swept tapered and untapered wings having a double wedge profile. Harmon and Swanson (Ref. 18) and Harmon (Ref. 19) applied the same methods to the evaluation of the wave drag for wings having a symmetrical biconvex profile. Chang (Ref. 20) applied the Von Karman integral method to the analysis of the flow about a general swept tapered planform wing at supersonic speed. The wave drag expressions, derived by these writers and used for the computation of drag values, are long and complicated. These formulae are published in available sources and are not, therefore, reproduced in this Handbook.

Reference is made here to a comprehensive survey by Lawrence (Ref. 21) of sources of supersonic drag theory. Drag data obtained from the original sources, supplemented by the results of additional computations, are presented in Lawrence (Ref. 21) in chart form for a wide range in planforms of double wedge and biconvex profile wings.

702.23 Discussion of the Curves for Lift, Moment, and Zero Lift Drag

Values of the lift-curve and the moment-curve slopes for a range of several commonly used finite wing planforms in supersonic flow have been computed at the Defense Research Laboratory of The University of Texas. These data are presented in the form of a modified lift-curve slope, βC_{L_α}, and a modified moment-curve slope, βC_{m_α}, plotted against $\beta \cot \Lambda$ for certain designated constant values of βA. The charts presenting values of the modified lift-curve slope, βC_{L_α}, are extended into the subsonic sweptforward trailing edge region by means of the reversibility theorem (see discussion in Subsection 702.3). Since this theorem does not apply to the moment characteristics, there is no data available for the moment-curve slope, βC_{m_α}, in the subsonic sweptforward trailing edge region. Lift-curve and moment-curve slopes for the subsonic sweptback trailing edge condition have not been obtained (see Subsection 702).

The zero lift pressure drag data for these wing planforms with symmetrical double wedge profiles are presented in this Handbook in the form of a Mach number-drag-thickness parameter, $\beta C_D / (\frac{t}{c})^2$. This parameter, $\beta C_D / (\frac{t}{c})^2$, is plotted versus $\beta \cot \Lambda$ for constant values of βA as was done for the C_{L_α} and C_{m_α} data.

The lift-curve slopes, the moment-curve slopes, and the data for pressure drag at zero lift for finite planforms where $\lambda = 0$, 0.5, 1.0, and trapezoidal wings are presented in Figs. 702.23-1 through 702.23-16. Similar data for rectangular wings can be found in Figs. 702.23-15 and 702.23-16 ($\tan \delta = 0$), and Fig. 702.23-12 ($\beta \cot \Lambda = \infty$). Composite diagrams showing the areas of solution for the lift-curve and moment-curve slope curves and drag curves of these planforms are included in this group of figures (Figs. 702.23-1, 702.23-5, 702.23-9, and 702.23-14). Primary reference sources for the data are cited in these figures for the convenience of the reader.

702.3 Reversibility Theorem

The assumptions of the linearized, potential-flow theory make possible the statement of a simple reversible flow theorem. Several authors have treated this problem under various restrictions (see Refs. 22 through 26). Brown, (Ref. 27) has shown that the lift-curve slope and the thickness drag remain the same when any airfoil, or system of airfoils, is reversed so long as the Kutta condition of finite velocity at the wing trailing edge applies. This theorem has enabled the extension of the data presented in this Handbook into certain areas not otherwise calculable. It allows one to determine the characteristics for those planforms which can be identified with an equivalent configuration for which the lift-curve slope and the thickness data are available in the Handbook. Examples illustrating these applications are included in the following subsections.

703 Numerical Examples

The evaluation of finite wing characteristics by the use of the data presented in this section of the Handbook is illustrated in the following examples.

703.1 Example 1: Wing with a Supersonic Leading and Trailing Edge

The determination of the theoretical lift-curve slope, the moment-curve slope, and the pressure drag coefficient for the following finite symmetrical double wedge wing is illustrated in this example.

Given:

Mach number	$M = 3.16$
Wing specifications	
Leading edge sweep angle	$\Lambda = 60°$
Thickness ratio	$\frac{t}{c} = 0.09$
Tip chord	$c_t = \frac{1}{2} c_r$
Wing span	$b = \frac{3}{2} c_r$

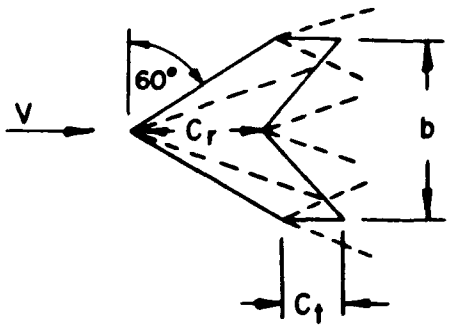

Computations:

$$\beta = \sqrt{M^2 - 1}$$
$$= 3.000$$
$$\cot \Lambda = 0.577$$
$$A = \frac{4}{3} \frac{b}{c_r}$$ (given from the geometry of the inset figure)
$$= 2$$
$$\text{Thus, } \beta A = 6.000$$
$$\text{and } \beta \cot \Lambda = 1.731$$

Figure 702.11-3 indicates supersonic leading and trailing edges.

$$\beta C_{L_\alpha} = 4.11 \text{ (from Fig. 702.23-6)}$$

$$\beta C_{m_\alpha} = -4.03 \text{ (from Fig. 702.23-7)}$$

$$\frac{\beta C_D}{(\frac{t}{c})^2} = 4.59 \text{ (from Fig. 702.23-8)}$$

Results:

$$C_{L_\alpha} = 1.37 \text{ per radian } (0.0239 \text{ per degree})$$

$$C_{m_\alpha} = -1.34 \text{ per radian } (-0.0234 \text{ per degree})$$

$$C_D = 0.0124$$

703.2 Example 2: Wing with a Supersonic Leading Edge and a Subsonic Trailing Edge

The determination of the theoretical lift-curve slope, the moment-curve slope, and the wave drag coefficient for a finite symmetrical double wedge wing is illustrated in this example.

Given:

Mach number	$M = 1.25$
Wing specifications	
Leading edge sweep angle	$\Lambda = 30°$
Thickness ratio	$\frac{t}{c} = 0.09$
Triangular panel	$\lambda = 0$
Wing span	$b = c_r$

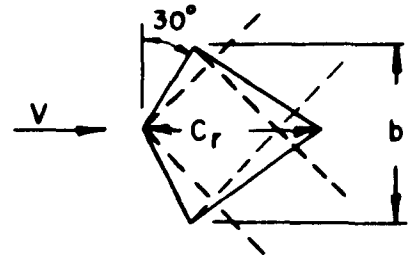

Computations:

$$\beta = \sqrt{M^2 - 1}$$
$$= 0.750$$
$$\beta \cot \Lambda = 1.732$$
$$A = \frac{2b}{c_r}$$ (given from the geometry of the inset figure)
$$= 2$$
Thus, $\beta A = 1.500$
and $\beta \cot \Lambda = 1.300$

Reference to Fig. 702.11-2 shows that this wing lies in the subsonic trailing edge region. Figure 702.23-1 indicates that the lift-curve slope and wave-drag coefficient can be computed by the application of the reversibility theorem referred to in Subsection 702.3.

This theorem simply states that the lift-curve slope and wave-drag coefficient given by the linearized theory for a given wing remain the same when the flow direction is rotated through 180 degrees, provided the Kutta condition at the trailing edge is satisfied. This condition is automatically satisfied for wings at zero lift as is true for the wing data presented herein.

The specified leading edge sweep angle of the wing in Example 2 is $\Lambda = 30°$ and $\lambda = 0$. The trailing edge sweep angle can be seen to be given as

$$\cot \Lambda_T = -0.703 .$$

The negative sign indicates a sweptforward trailing edge for the specified wing and therefore the reverse flow wing would have a sweptback leading edge. The computations for the reverse flow wing are made in the following manner.

703.21 Use of the Reversibility Theorem to Extend the Curves

Reverse flow wing computations:

$\beta \cot \Lambda = 0.527$

$\beta A = 1.500$

$\beta C_{L_\alpha} = 2.41$ (from Fig. 702.23-2)

βC_{m_α} = reversibility theorem not applicable

$\frac{\beta C_D}{(\frac{t}{c})^2} = 3.74$ (from Fig. 702.23-4)

$C_{L_\alpha} = 3.21$ per radian (0.054 per degree)

$C_D = 0.0404$

The curves in Figs. 702.23-2 and 702.23-4 have been extended into the subsonic trailing edge region by the method illustrated in this example.

703.3 Example 3: Wing with a Sweptforward Leading Edge

The determination of the theoretical lift-curve slope and the wave-drag coefficient for wings with a sweptforward leading edge is illustrated in this example. These data are obtained by computations for the equivalent reverse flow wing as demonstrated by the reversibility theorem:

Given:

Mach number $M = 1.80$

Wing specifications

Leading edge sweep angle $\Lambda = -45°$

Thickness ratio $\frac{t}{c} = 0.09$

Tip chord $c_t = \frac{1}{2} c_r$

Wing span $b = \frac{3}{2} c_r$

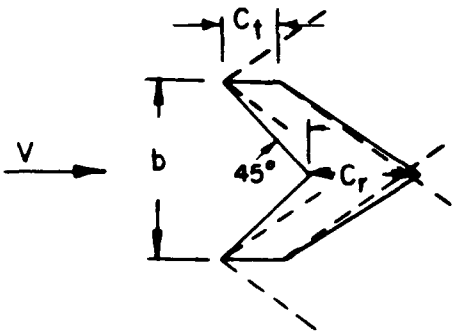

Computations:

$\cot \Lambda = -1.00$

From the given values of Λ and λ,

$\cot \Lambda_T = -0.60$

489030 O - 59 - 3

Since $\cot \Lambda_T$ is negative (thereby indicating a sweptforward trailing edge) the equivalent reverse flow wing would have a sweptback leading edge. The computations for the equivalent reverse flow wing are made in the following subsection.

703.31 Reverse Flow Wing

Computations:

$$\beta = \sqrt{M^2 - 1}$$

$$= 1.500$$

$$A = \frac{4}{3}\frac{b}{c_r} \quad \text{(given from the geometry of the inset figure)}$$

$$= 2$$

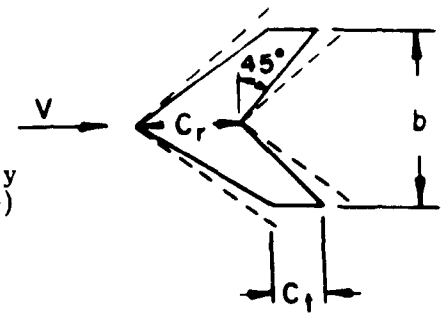

Thus, $\beta A = 3.00$

$\beta \cot \Lambda = 0.900$

and $\beta C_{L_\alpha} = 3.47$ (from Fig. 702.23-6)

$\frac{\beta C_D}{(\frac{t}{c})^2} = 5.35$ (from Fig. 702.23-8)

Results:

$C_{L_\alpha} = 2.31$ per radian (0.0403 per degree)

$C_D = 0.0289$

704 Comparison of Theory and Experiment

A systematic comparison of the measured and the theoretically calculated aerodynamic characteristics of a large number of finite wings at supersonic speeds has been made by Vincenti at the Ames Aeronautical Laboratory of the National Advisory Committee for Aeronautics (Ref. 28). Approximately thirty wing models were tested at a Mach number of 1.53 in the experimental investigation in which the lift, pitching-moment, and drag characteristics were determined. Figures 704-1 through 704-6 in this section of the Handbook present a graphical summary of these results based on Figs. 4 through 9 of the reference cited above. The comparisons given in these figures should give a convenient basis for estimating the accuracy and reliability of engineering predictions from the linearized theory.

Comparisons of lift-curve slopes as determined by measurement and theory for variations in aspect ratio and sweep angle are shown in Figs. 704-1 and 704-2. The wings in these instances had isosceles triangle sections of 5 per cent maximum thickness. The agreement with respect to aspect ratio is so good that Vincenti suggests that the effects of viscosity and support-interference must be almost completely compensating for the wings tested. The trends in the effects of sweep on the lift-curve slopes (Fig. 704-2) as predicted by the linear theory are, therefore, confirmed by the experimental results. The symmetry of the lift-curve slope with variation in sweep angle verifies the theoretically predicted invariance of the lift-curve slope with the flow direction reversed. However, the generally acceptable agreement in over-all lift characteristics must not be construed to imply satisfactory agreement with regard to load distribution.

Similar comparisons for the moment-curve slope are shown in Figs. 704-3 and 704-4. The agreement in these instances is neither qualitatively nor quantitatively good. The lack of symmetry with respect to sweepback and sweepforward (Fig. 704-4) verifies the nonreversibility prediction for moment characteristics. Vincenti suggests that the development of second-order wing theory may be necessary for solution of the pitching-moment prediction problem.

The effect of variation in sweep on the minimum drag is shown in Fig. 704-5. Again the symmetry verifies the conclusions of reversibility theorems. The amount of the increase in drag with increase in sweep predicted by linear theory is not observed experimentally. The difference between the measured and theoretical drag at low sweep angles is consistent with a reasonable estimation of the friction drag which must be added to the theoretical wave drag to obtain the total drag. However, it appears on the same basis that linear theory predicts too high a drag as the wing sweep approaches coincidence with the Mach line direction. Theoretical results for the subsonic trailing edge condition are not available, but the generally predicted reduction in drag as the wing is swept behind the Mach cone is verified by the experimental results. Figure 704-6 shows a comparison for results on double wedge profile triangular wings of varying maximum thickness position. The addition of an estimated skin friction to the wave drag produced a reasonably satisfactory agreement.

It must be concluded, therefore, that linearized theory data can be used only as a general guide for design predictions.

705 Limitations of the Linearized Theory

The effect of viscosity, the effect of wing-body interference, and higher order corrections to the linearized theory must be accounted for in any design applications. The reader is referred to Hilton (Ref. 29) and Shapiro (Ref. 30) for a more general discussion of the three-dimensional wing problem at supersonic speeds.

705.1 The Effect of Viscosity

The drag data presented in this section do not include any viscous effects. In the absence of reliable experimental information on wing drag at supersonic speeds, a useful estimation can be arrived at by the addition of a calculated average skin friction coefficient such as presented in Section 6 of the Handbook (Two-Dimensional Airfoils).

705.2 Wing-Body Interference

An important factor which is always present to modify the predicted summation of characteristics from the component parts is wing-body interference effects. In general, the evaluation of these effects must be obtained through precise experimental and analytical studies. The importance and extensiveness of this subject warrants its presentation in a separate section of the Handbook (Section 9: Mutual Interference Phenomena) where this problem is discussed in detail.

705.3 Higher Order Theories

The need for second order theory for finite wings at supersonic speeds was suggested earlier as a result of the unsatisfactory prediction of pitching-moment (see Subsection 704 and Figs. 704-3 and 704-4). The usefulness of extending the first order theory to a higher order theory is somewhat questionable because of the possible presence of large viscous effects. The magnitude of the effects of higher order approximations in two-dimensional flows is thoroughly treated in Section 6 of the Handbook (Two-Dimensional Airfoils).

Van Dyke (Ref. 31) discusses the development of a second order theory in some detail, and Lighthill (Ref. 35) presents a general discussion of higher order approximations for supersonic three-dimensional wing theory. However, results of immediate interest, beyond those of the linearized theory, do not appear to be available.

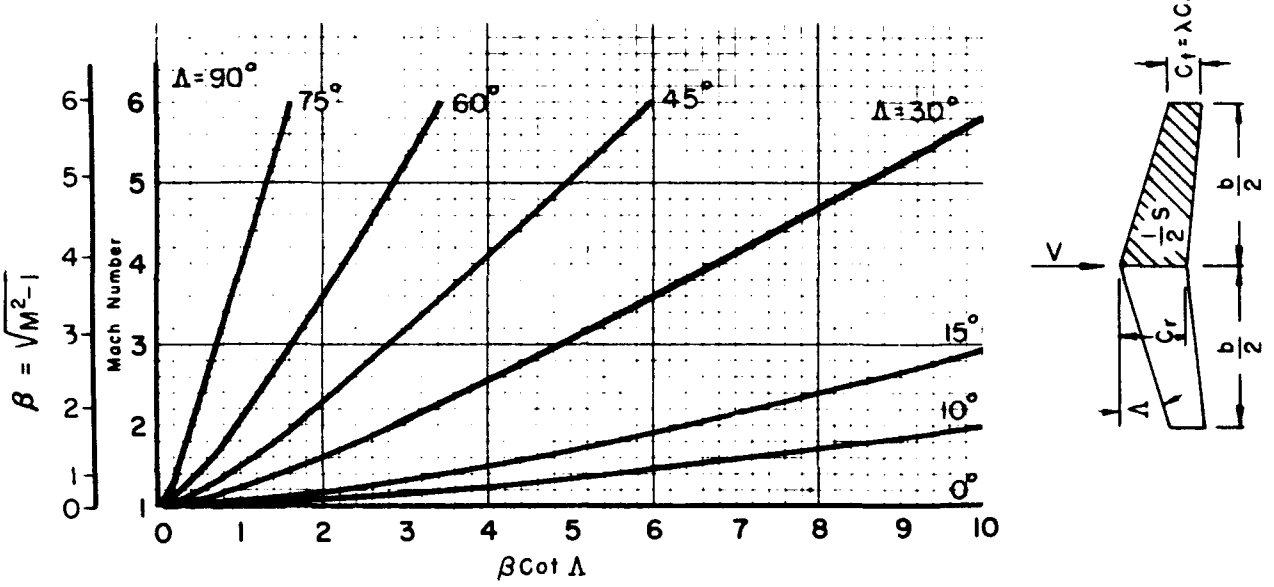

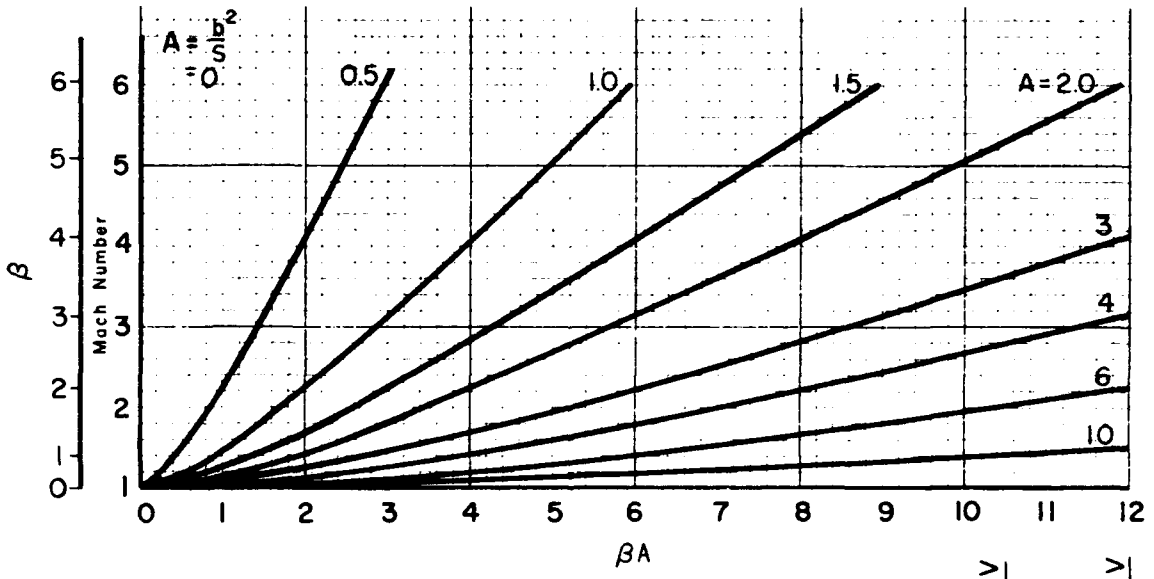

Trailing Edge Sweptback	$\beta A > 4\frac{1-\lambda}{1+\lambda}$	β Cot Λ
Trailing Edge Unswept	$\beta A = 4\frac{1-\lambda}{1+\lambda}$	β Cot Λ
Trailing Edge Sweptforward	$\beta A < 4\frac{1-\lambda}{1+\lambda}$	β Cot Λ
Double Symmetrical Planform	$\beta A = 2\frac{1-\lambda}{1+\lambda}$	β Cot Λ

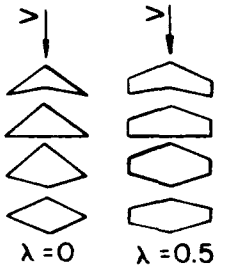

702.11 Figure 1 Variation of βA and $\beta \cot \Lambda$ with Mach Number, M, for constant values of aspect ratio, A, and sweepback angle, Λ.

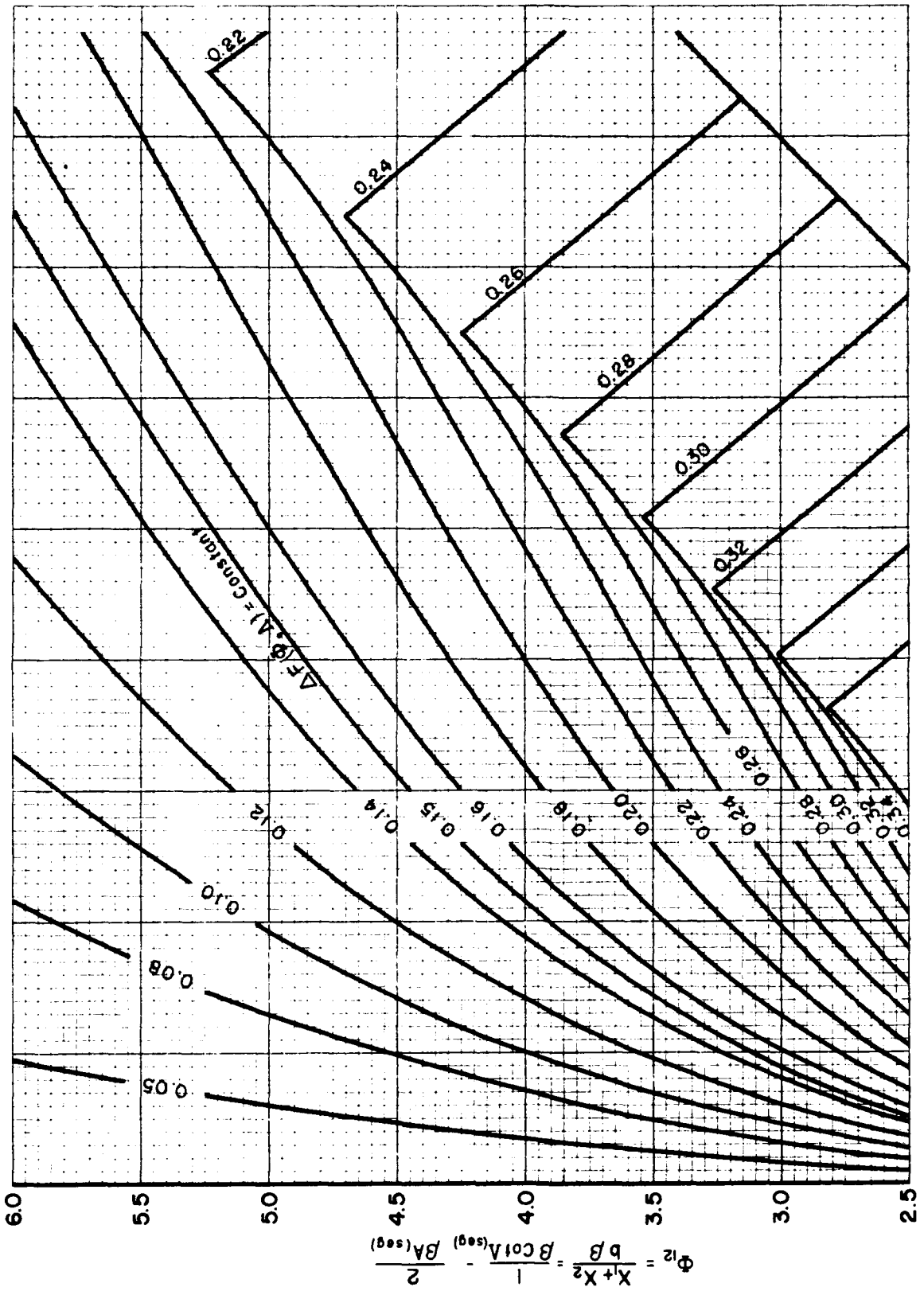
0.22
0.24
0.26
0.28
0.30
0.32
ΔF(β, A) = constant
0.05
0.08
0.10
0.12
0.14
0.16
0.18
0.20
0.22
0.24
0.26
0.28
0.30
0.32
0.34
6.0
5.5
5.0
4.5
4.0
3.5
3.0
2.5
$\Phi_{12} = \frac{X_1 + X_2}{b\,\beta} = \frac{1}{\beta \cot \Lambda_{(sea)}} - \frac{2}{\beta A_{(sea)}}$

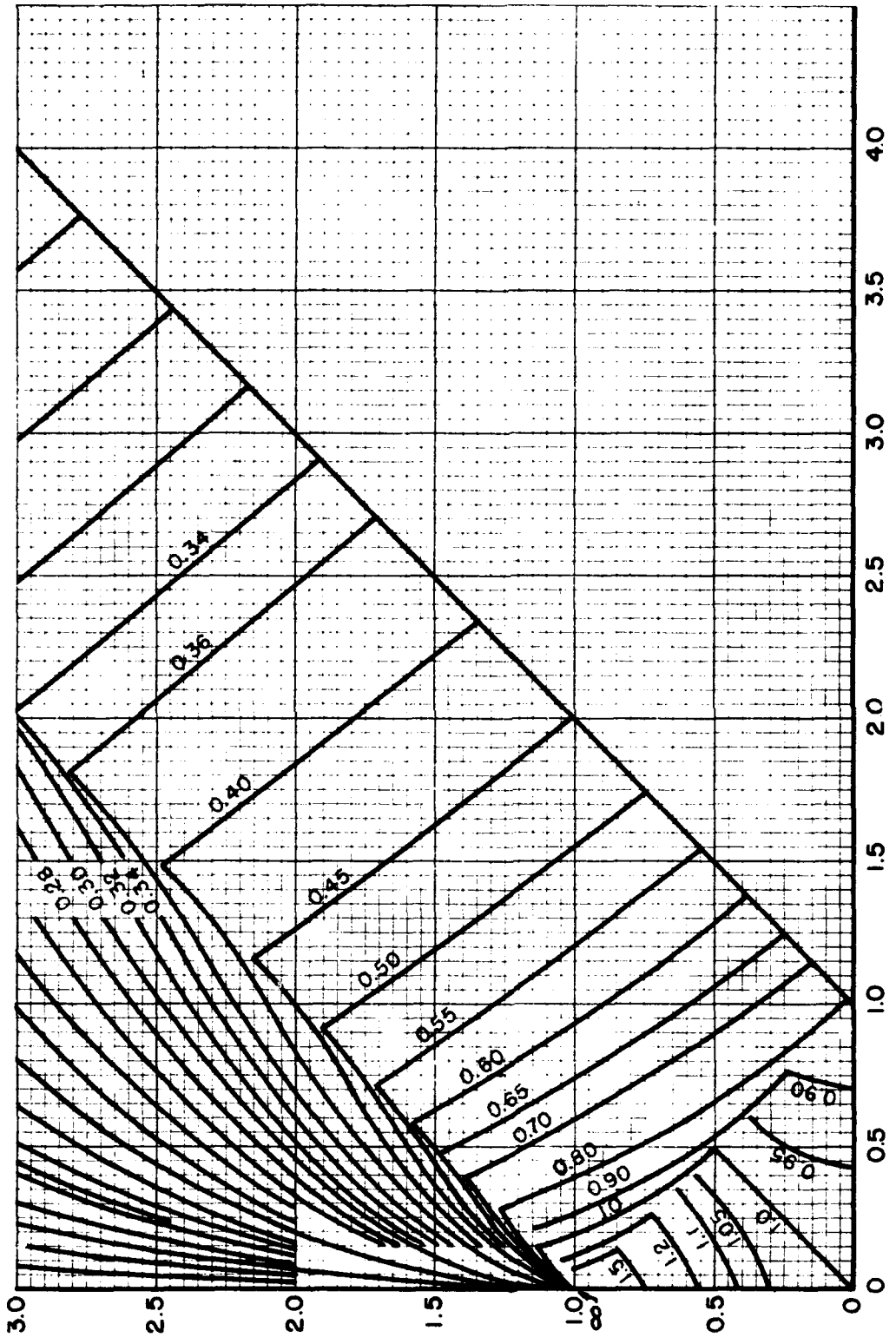

$$\Lambda_{12} = \frac{X_1 - X_2}{b\beta} = \frac{2}{\beta A_{(leg)}}$$

702.22 Figure 1 Chart for the function ΔF to be used in the calculation of pressure drag of $\lambda = 0$ planforms (Taken from Ref. 36).

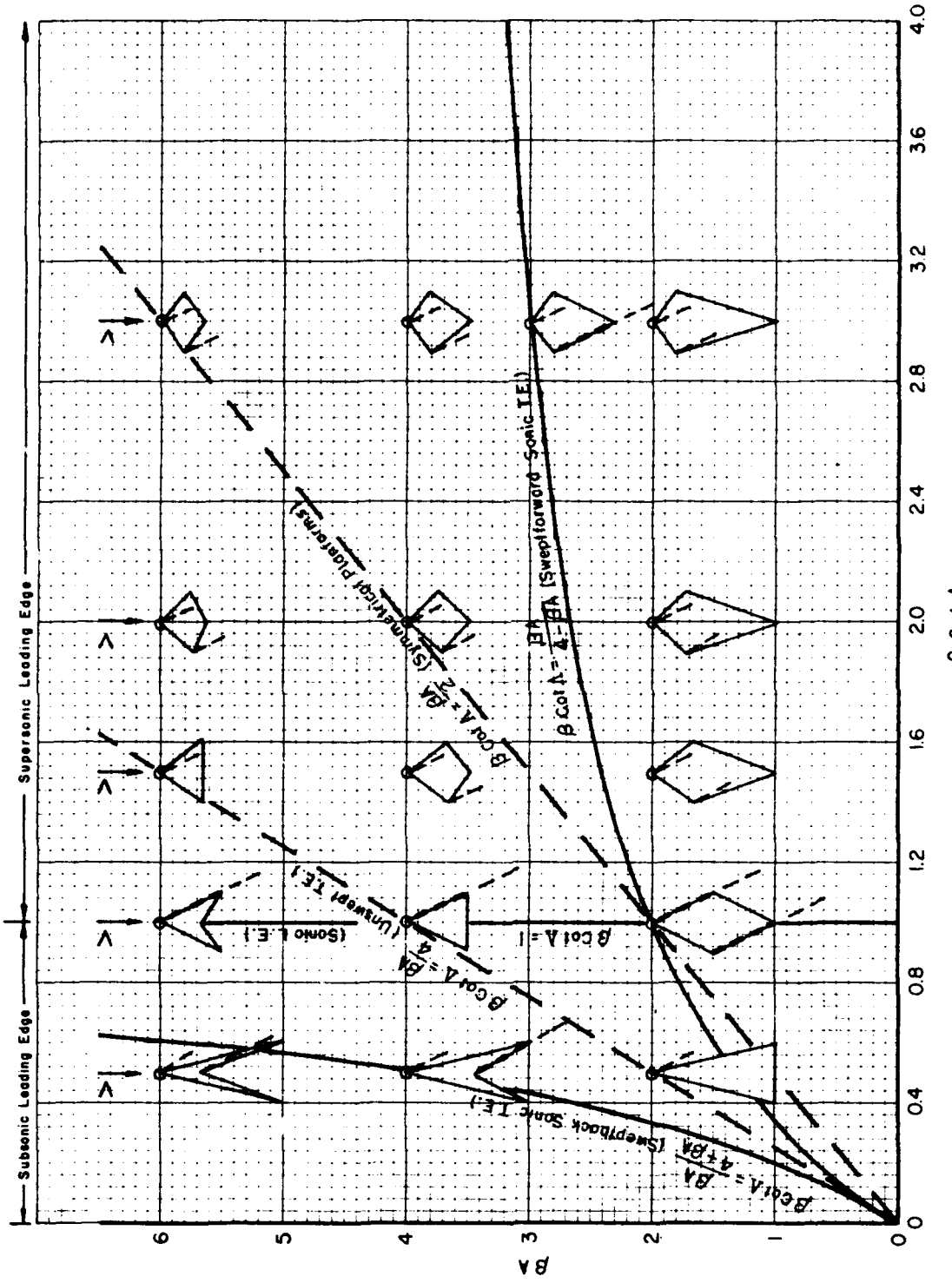

702.11 Figure 2 Variations in planform associated with changes in the planform parameters, βA and $\beta \cot \Lambda$; $\lambda = 0$.

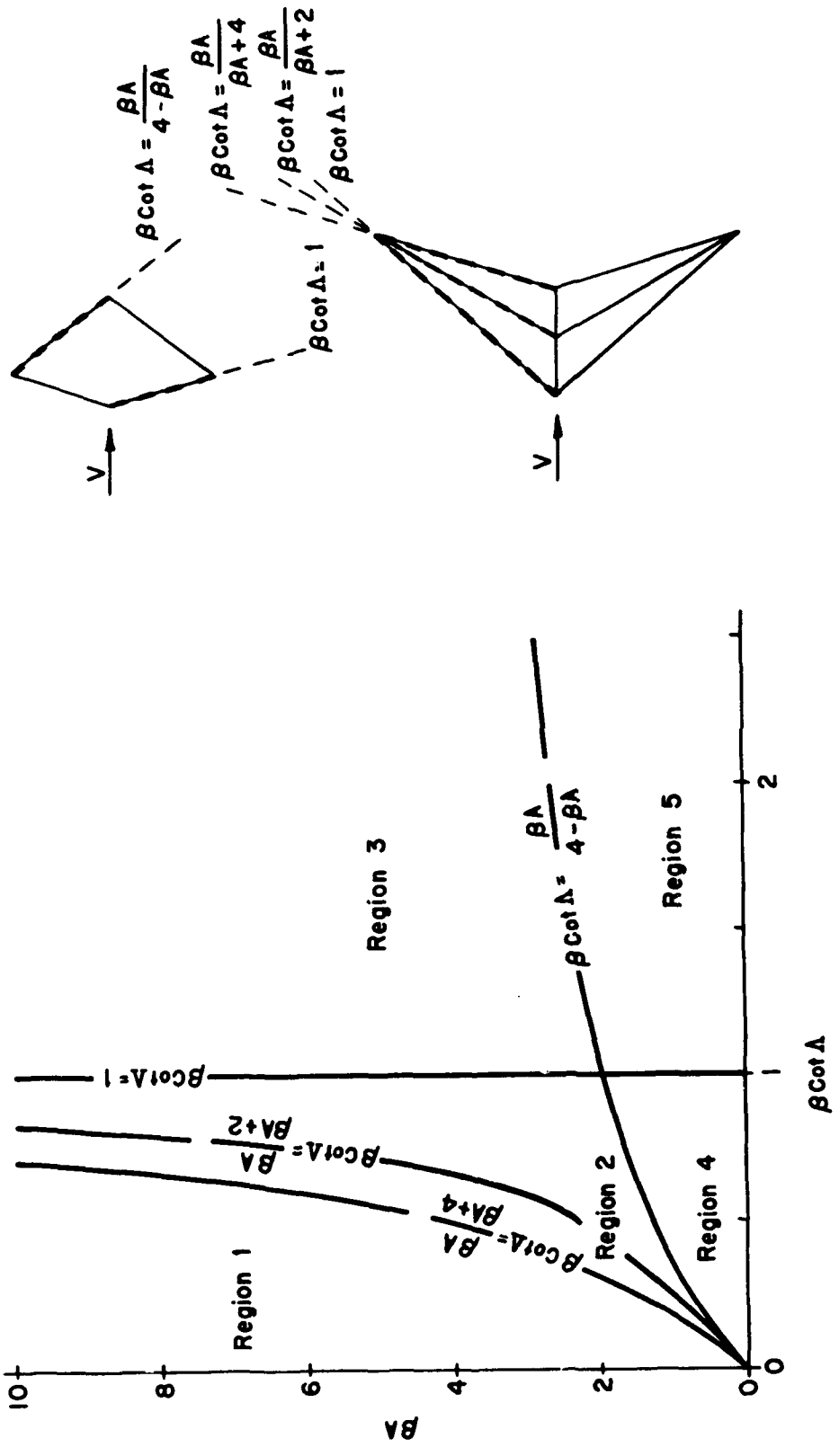

702.23 Figure 1 Composite diagram showing the areas of solution and primary reference sources for the lift, moment, and drag curves, $\lambda = 0$.

	Region	Source References
C_{L_α}	1,4	No solution obtained. Trailing edge is subsonic.
	2	Replotted from DRL, Eq. 704.12 (Ref. 12). Taken from Piland, Eq. 14 (Ref. 11).
	3	Replotted from DRL, Eq. 704.14 (Ref. 12). Taken from Piland, Eq. 17 (Ref. 11).
	5	Solution obtained by use of reversibility theorem.
C_{m_α}	1,4,5	No solution obtained. Trailing edge is subsonic.
	2	Replotted from DRL, Eq. 704.13b (Ref. 12). Taken from Piland, Eq. 15 (Ref. 11).
	3	Replotted from DRL, Eq. 704.15 (Ref. 12) by use of the method in Cohen (Ref. 32).
C_D	1,2,3	Replotted from Lawrence (Ref. 21). Based on the charts of Multhopp and Winter (Ref. 36).
	4	No solution obtained.
	5	Solution obtainable by use of the reversibility theorem.

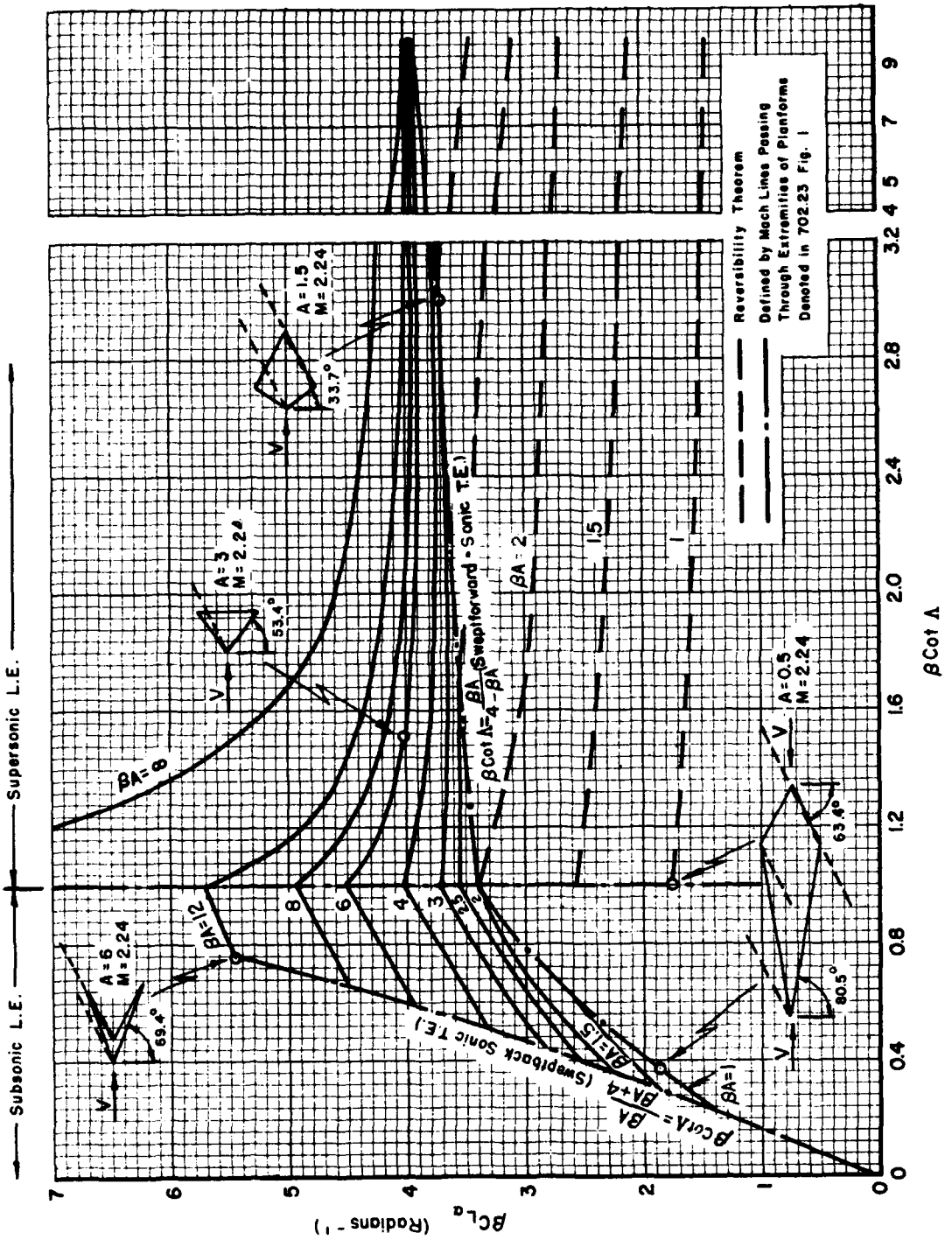

702.23 Figure 2 Generalized curves of the wing lift-curve-slope parameter for tapered wings with swept leading edges, $\lambda = 0$.

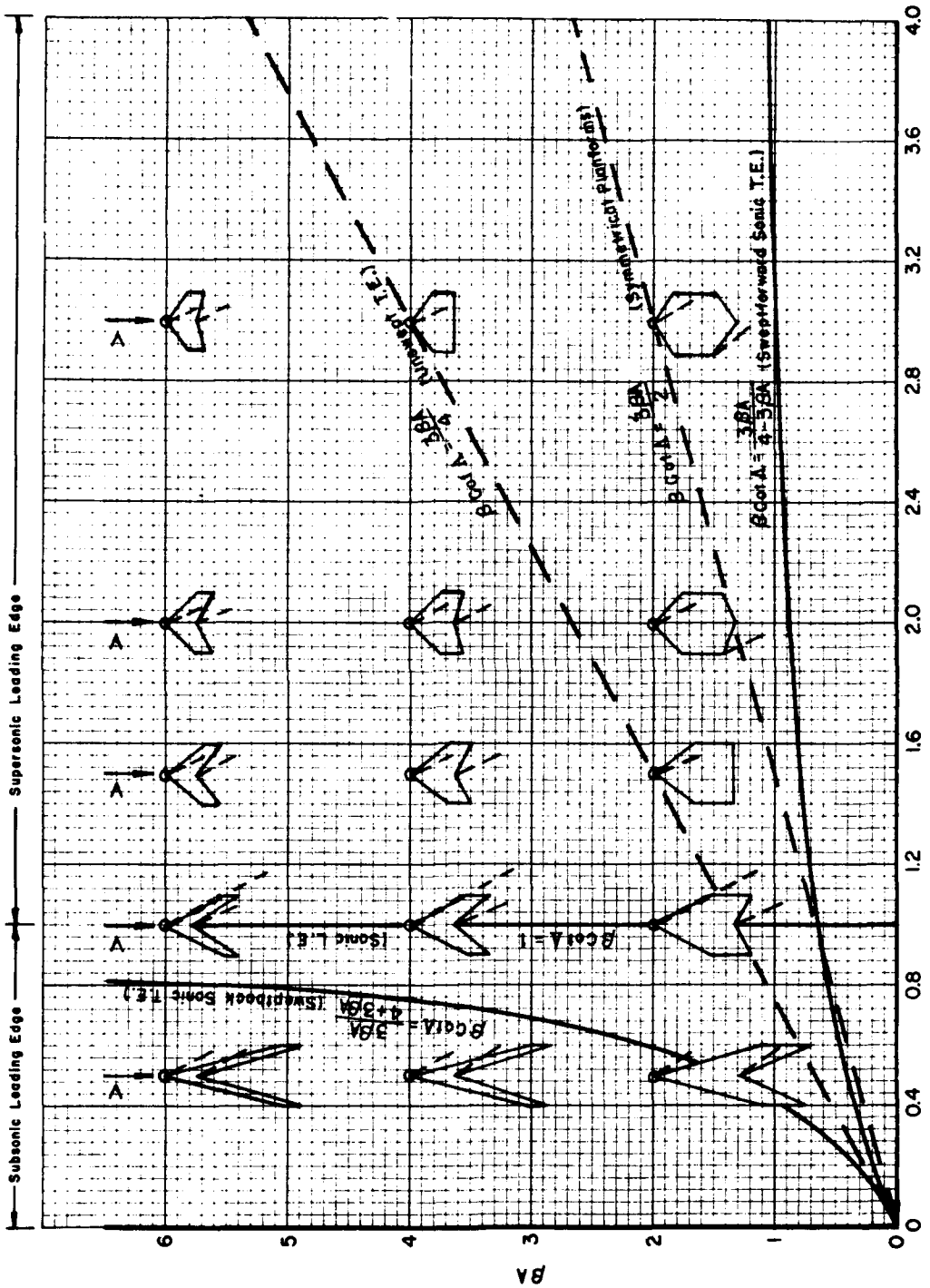

702.11 Figure 3 Variations in planform associated with changes in the planform parameters, βA and $\beta \cot \Lambda$; $\lambda = 0.5$.

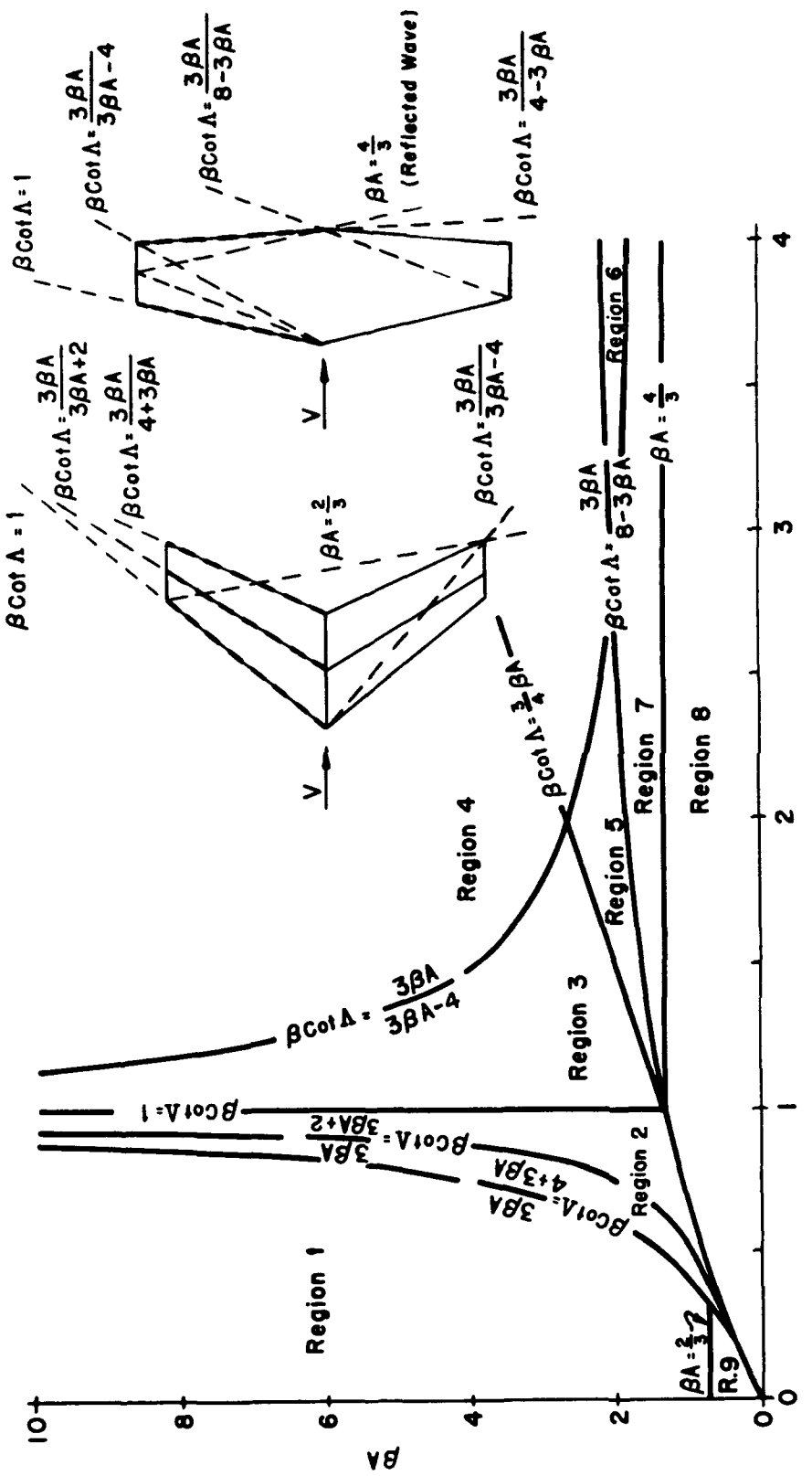

702.23 Figure 5 Composite diagram showing the areas of solution and primary reference sources for the lift, moment, and drag curves, $\lambda = 0.5$.

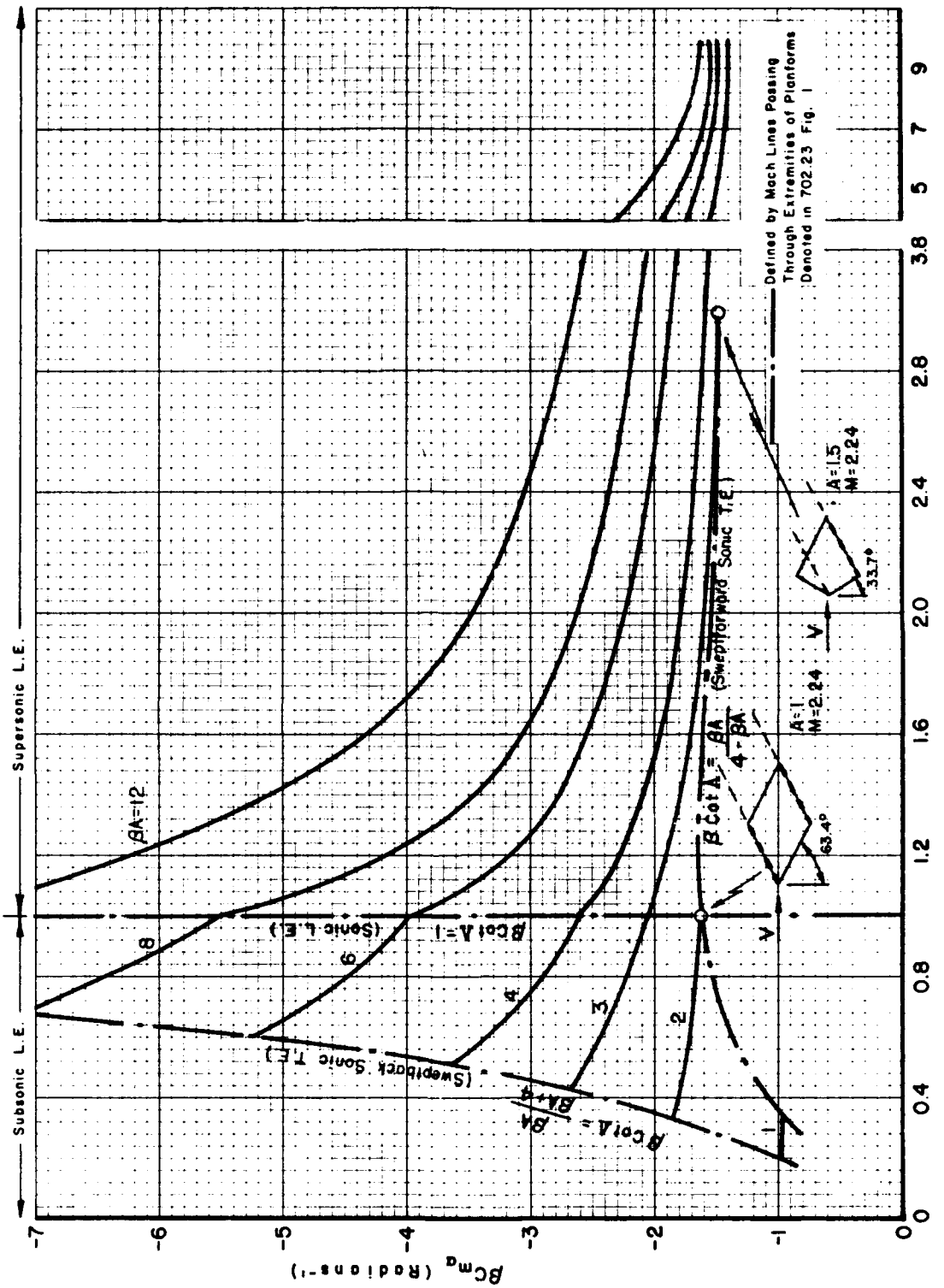

702.23 Figure 3 Generalized curves of the wing moment-curve-slope parameter for tapered wings with swept leading edges, λ = 0.

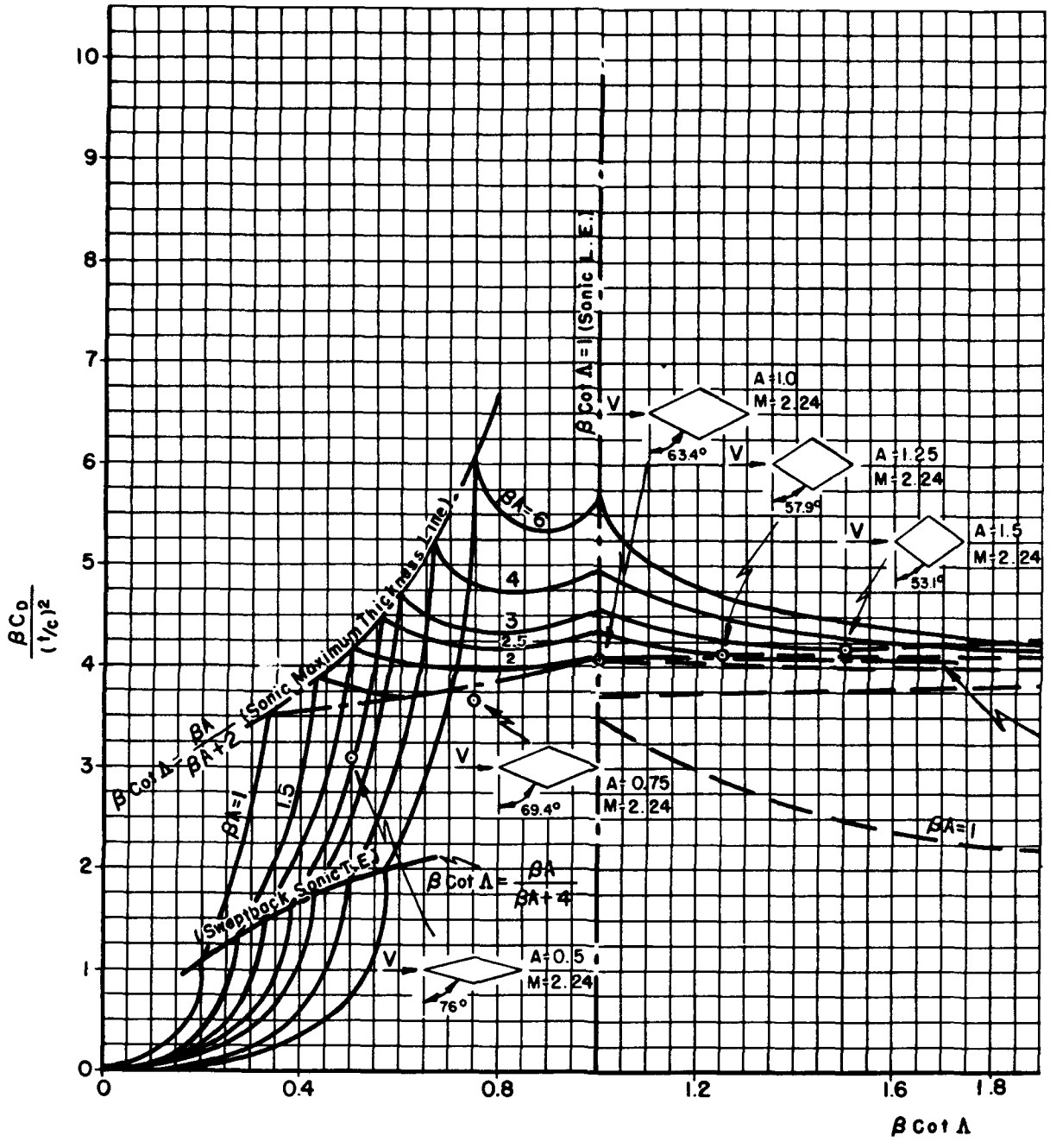

702.23 Figure 4 Generalized curves of the wing pressure-drag parameter at zero lift for tapered wings with

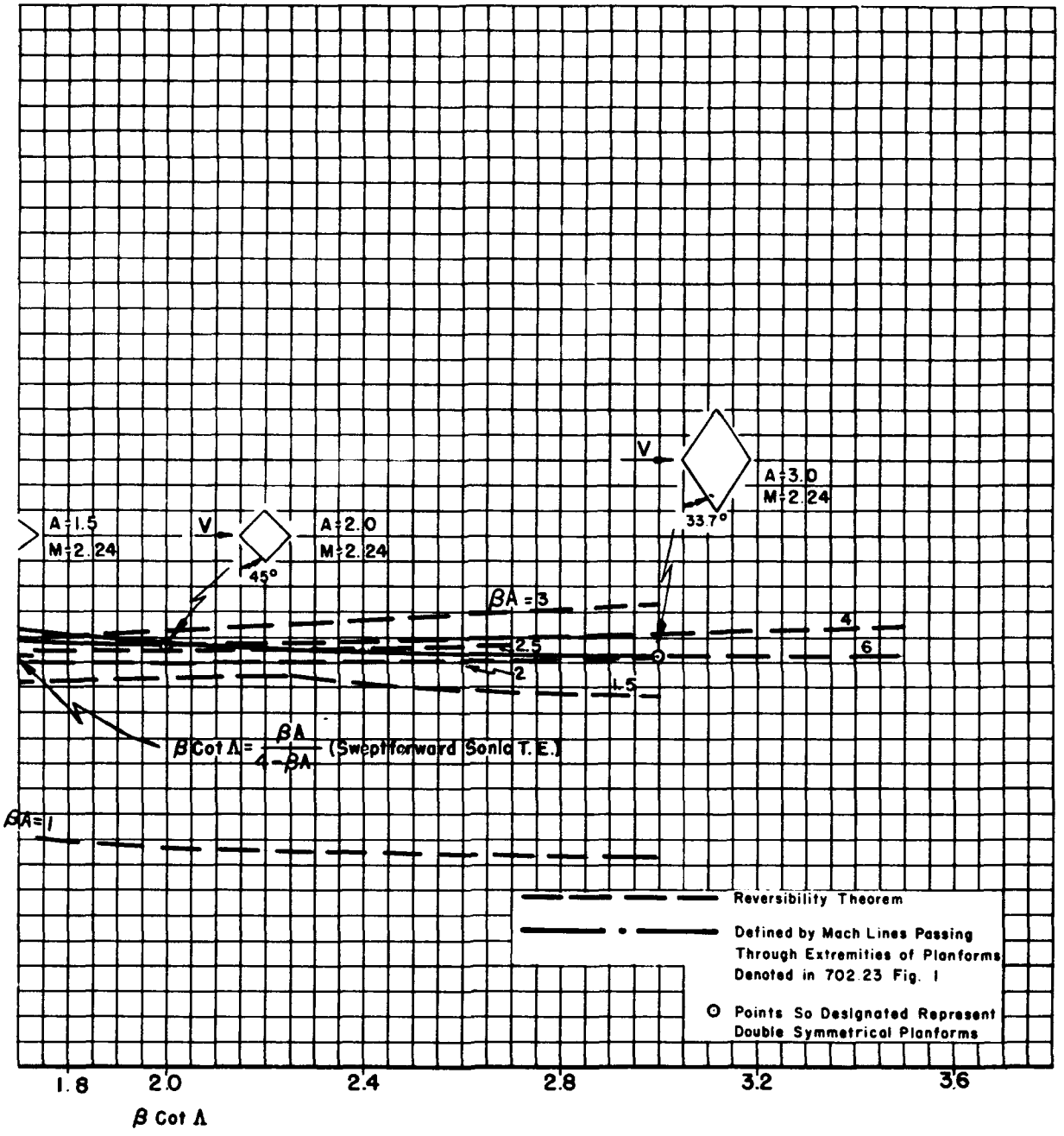

swept leading edges; double wedge profile, maximum thickness at 0.5 chord, λ = 0.

489030 O - 59 - 4

	Region	Source References
C_{L_α}	1, 9	No solution obtained. Trailing edge is subsonic.
	2	Replotted from DRL, Eq. 704.16 (Ref. 12). Taken from Piland, Eq. 23 (Ref. 11).
	3, 5	Replotted from DRL, Eq. 704.18 (Ref. 12). Taken from Cohen, Eqs. 5 and 31 (Ref. 32) and Lapin, Table VI, Eqs. I-11 and II-2 (Ref. 34).
	4	Replotted from DRL, Eq. 704.20 (Ref. 12). Taken from Piland, Eq. 25 (Ref. 11).
	6	Solution obtainable by use of the reversibility theorem.
	7, 8	No solution obtained. Mach wave from wing tip intersects opposite wing panel.
C_{m_α}	1, 2, 9	No solution obtained. Leading edge is subsonic.
	3, 5	Replotted from DRL, Eq. 704.19b (Ref. 12) by use of the method in Cohen (Ref. 32).
	4	Replotted from DRL, Eq. 704.21c (Ref. 12) by use of the method in Cohen (Ref. 32).
	6	No solution obtained.
	7	Obtainable from DRL, Eq. 704.17c (Ref. 12) by use of the method in Cohen (Ref. 32).
	8	No solution obtained. Leading edge is subsonic, or Mach wave from wing apex is reflected from wing tip onto opposite wing panel.
C_D	1, 2, 3, 4, 5	Replotted from Lawrence (Ref. 21). Based on the work of Margolis (Ref. 17) and Chang (Ref. 20).
	7	Solution obtained only for planforms with fore-aft symmetry (see Nielsen, Ref. 38). No other solution obtained. Mach wave from wing tip intersects opposite wing panel.
	9	No solution obtained. Mach wave from wing tip intersects opposite wing panel.
	6, 8	Solution obtainable by use of the reversibility theorem in region 6 and in a limited portion of region 8.

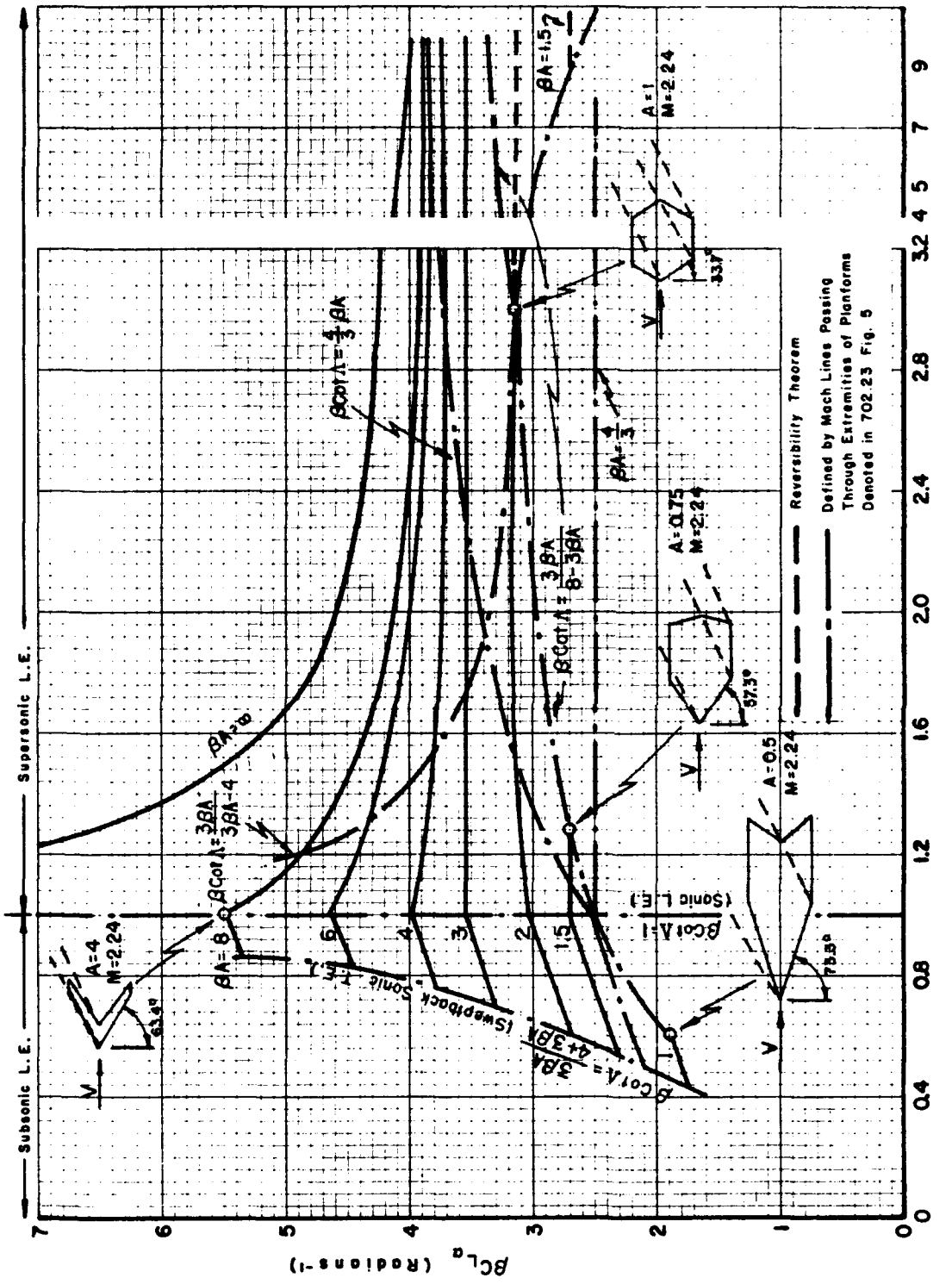

702.23 Figure 6 Generalized curves of the wing lift-curve-slope parameter for tapered wings with swept leading edges, $\lambda = 0.5$.

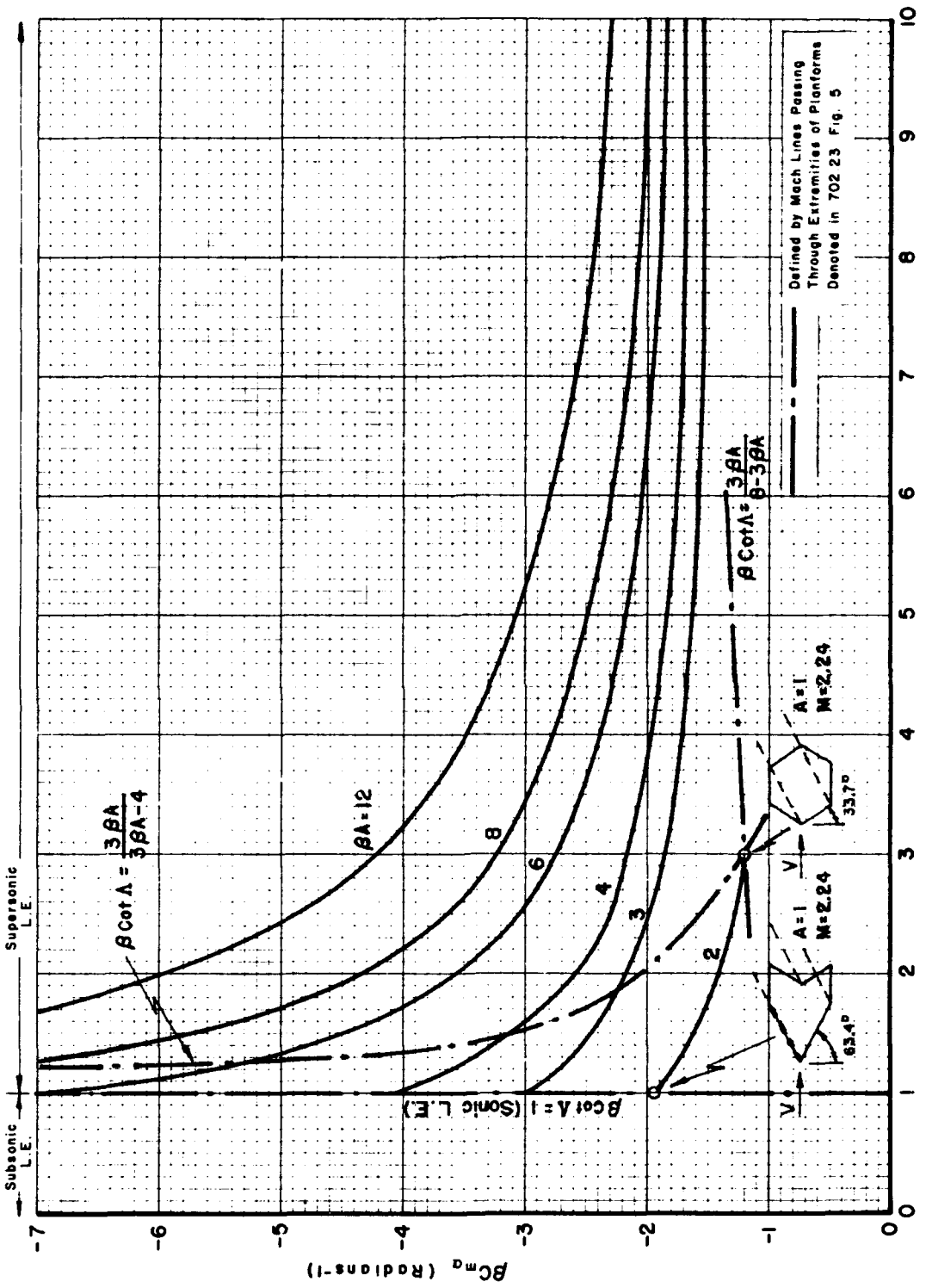

702.23 Figure 7 Generalized curves of the wing moment-curve-slope parameter for tapered wings with swept leading edges, λ = 0.5.

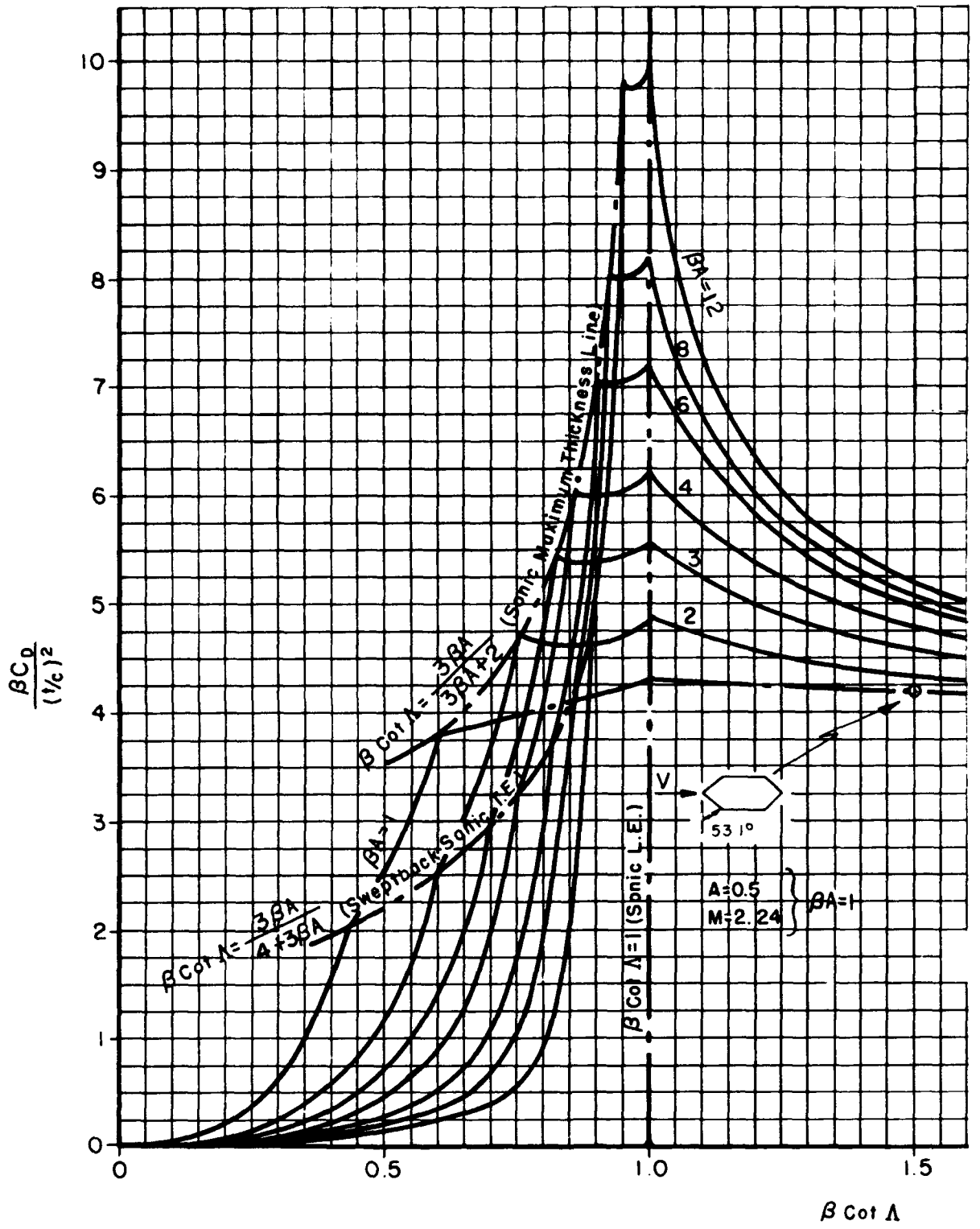

702.23 Figure 8 Generalized curves of the wing pressure-drag parameter at zero lift for tapered wings with

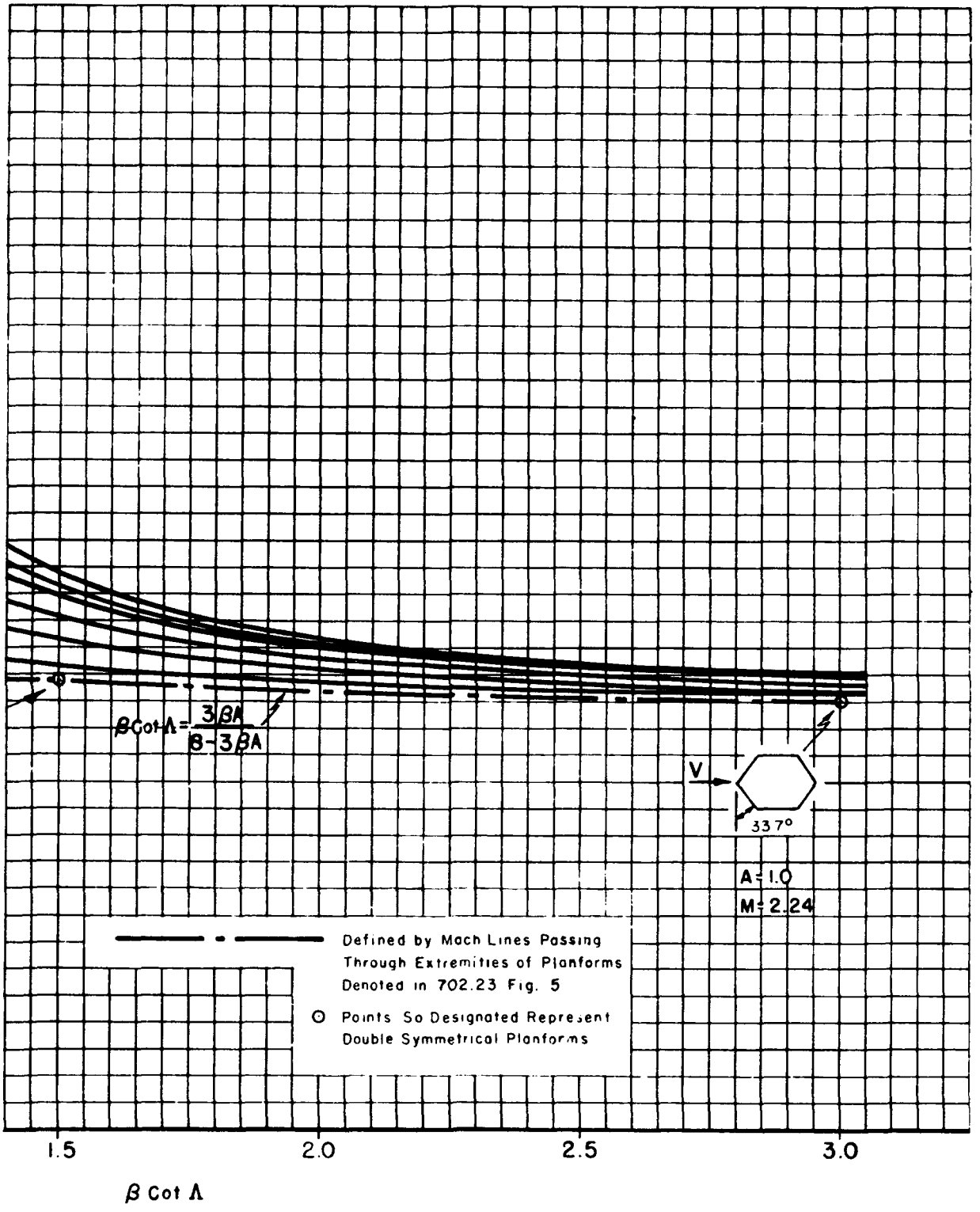

swept leading edges; double wedge profile, maximum thickness at 0.5 chord, λ = 0.5.

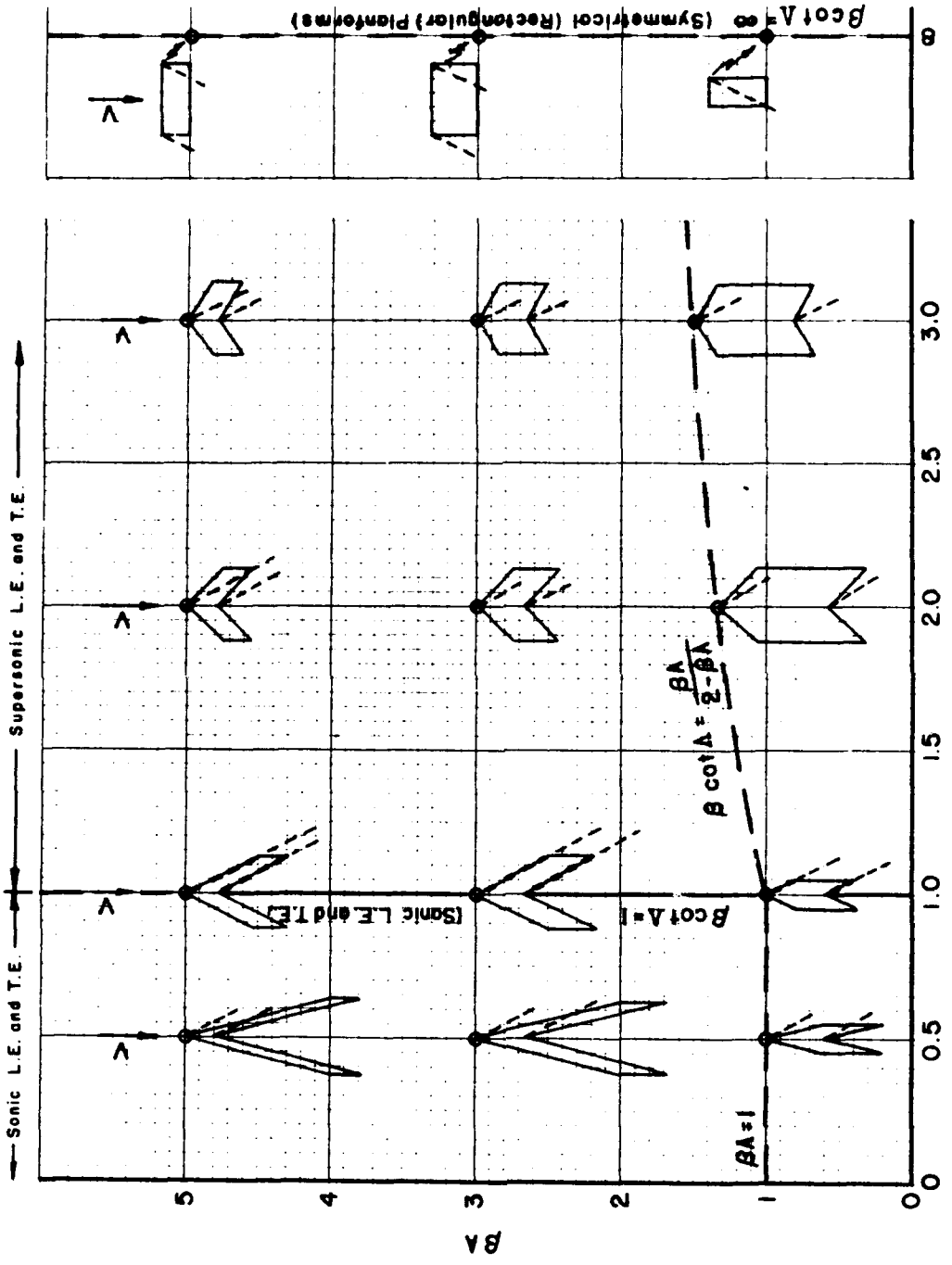

702.11 Fig. 4 Variations in planform associated with changes in the planform parameters βA and $\beta \cot \Lambda$; $\lambda = 1.0$

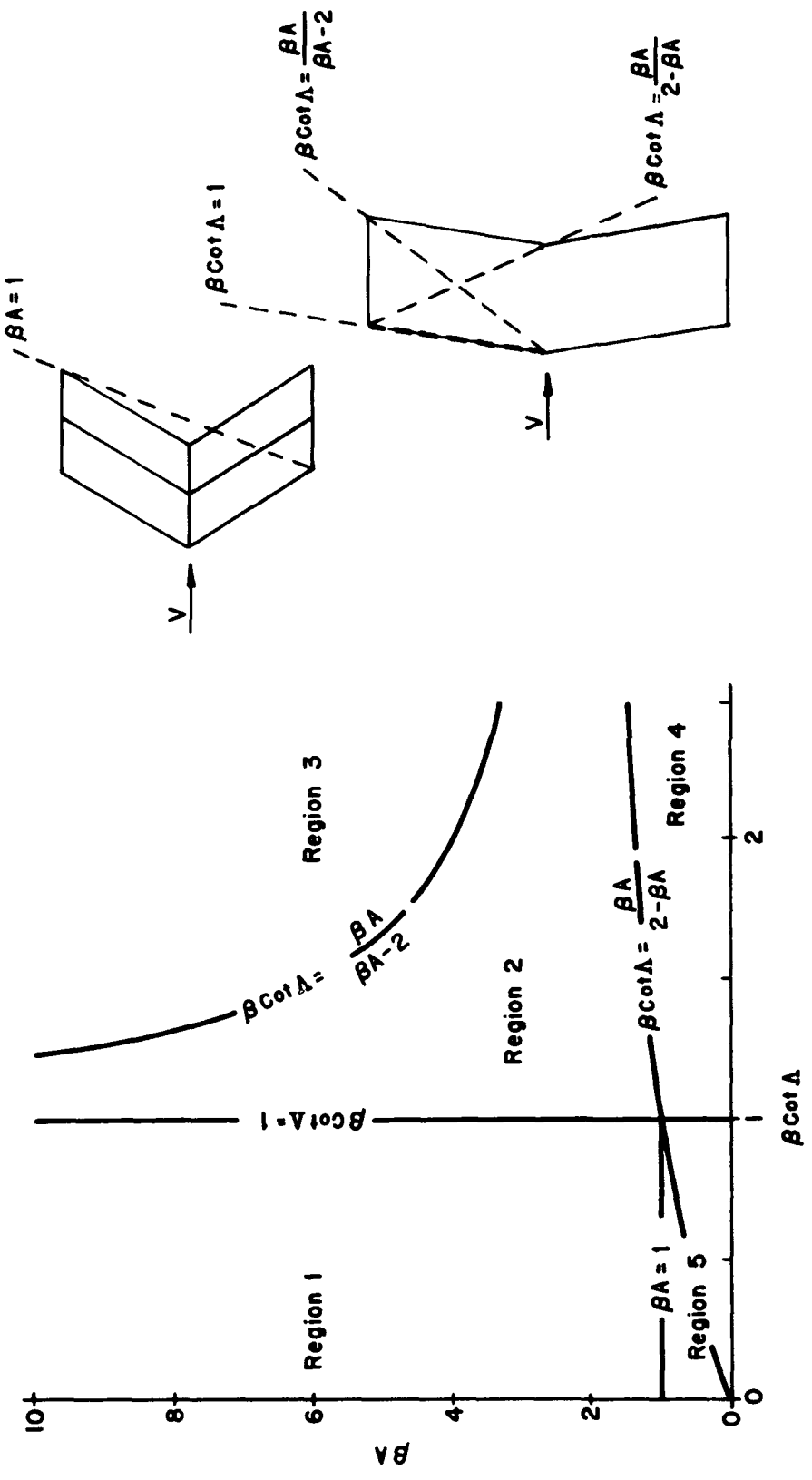

702.23 Figure 9 Composite diagram showing the areas of solution and primary reference sources for the lift, moment, and drag curves, $\lambda = 1.0$.

	Region	Source References
C_{L_α}	1, 5	No solution obtained. Sweptback leading and trailing edges are subsonic.
	2	Replotted from DRL, Eq. 704.8 (Ref. 12). Taken from Cohen, Eqs. 6 and 32 (Ref. 32) and Piland, Eq. 21 (Ref. 11).
	3	Replotted from DRL, Eq. 704.10 (Ref. 12). Taken from Cohen, Eqs. 6 and 32 (Ref. 32) and Piland, Eq. 21 (Ref. 11).
	4	Solution obtained for $\cot \Lambda = \infty$ (rectangular wing). See Region 4, Fig. 702.23-14. No other solutions obtained. Mach wave from tip crosses opposite trailing edge.
C_{m_α}	1, 5	No solution obtained. Sweptback leading and trailing edges are subsonic.
	2	Replotted from DRL, Eq. 704.9d (Ref. 12). Based on Cohen, Eqs. 9 and 34 (Ref. 32).
	3	Replotted from DRL, Eq. 704.11c (Ref. 12) by use of the method in Cohen (Ref. 32).
	4	Solution obtained for $\cot \Lambda = \infty$ (rectangular wing). See Region 4, Fig. 702.23-14. No other solutions obtained. Mach wave from tip crosses opposite trailing edge.
C_D (double wedge)	1, 2, 3	Replotted from Lawrence (Ref. 21) and based on the work of Margolis (Ref. 16).
	4, 5	Solution obtained for $\cot \Lambda = \infty$ (rectangular wing) for $\beta A \geq 1/2$ (Ref. 38). No other solutions obtained. Mach wave from tip crosses opposite trailing edge.
C_D (biconvex)	1, 5	Replotted from Lawrence (Ref. 21) and based on the work of Harmon and Swanson (Ref. 18).
	2, 3, 4	Replotted from Lawrence (Ref. 21) and based on the work of Harmon (Ref. 19).

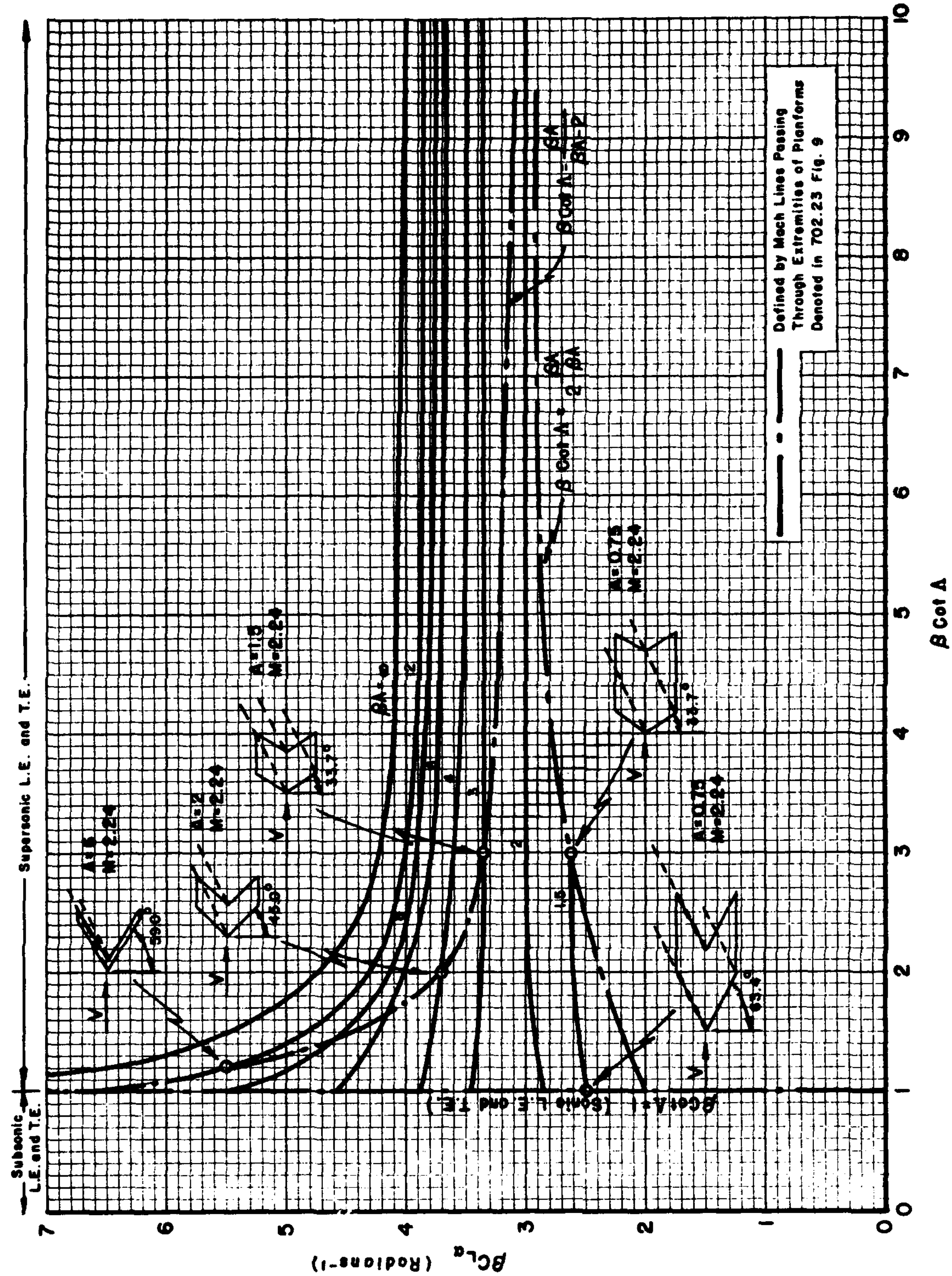

702.23 Figure 10 Generalized curves of the wing lift-curve-slope parameter for untapered wings with swept leading edges, $\lambda = 1.0$.

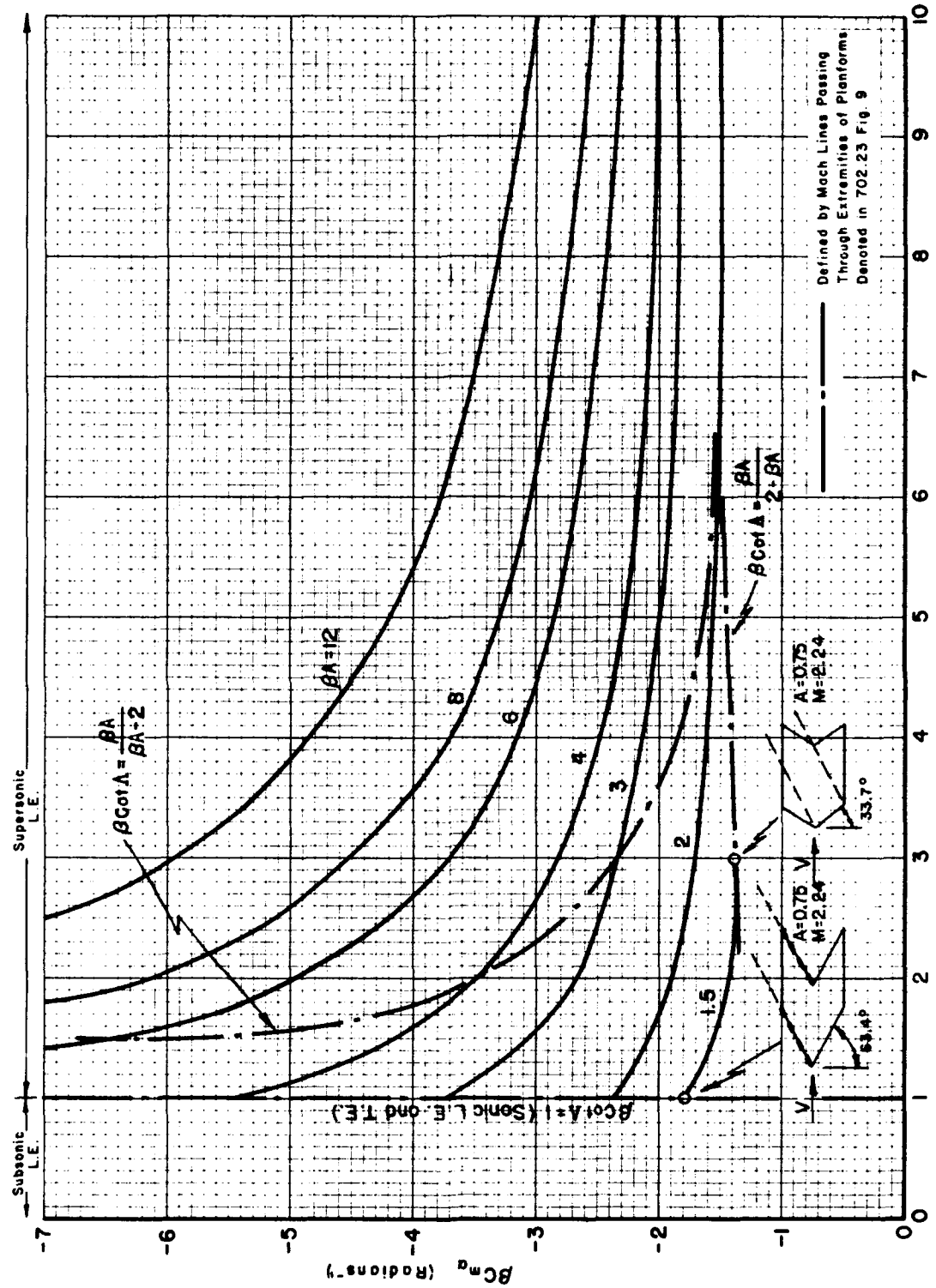

702.23 Figure 11 Generalized curves of the wing moment-curve-slope parameter for untapered wings with swept leading edges, λ = 1.0.

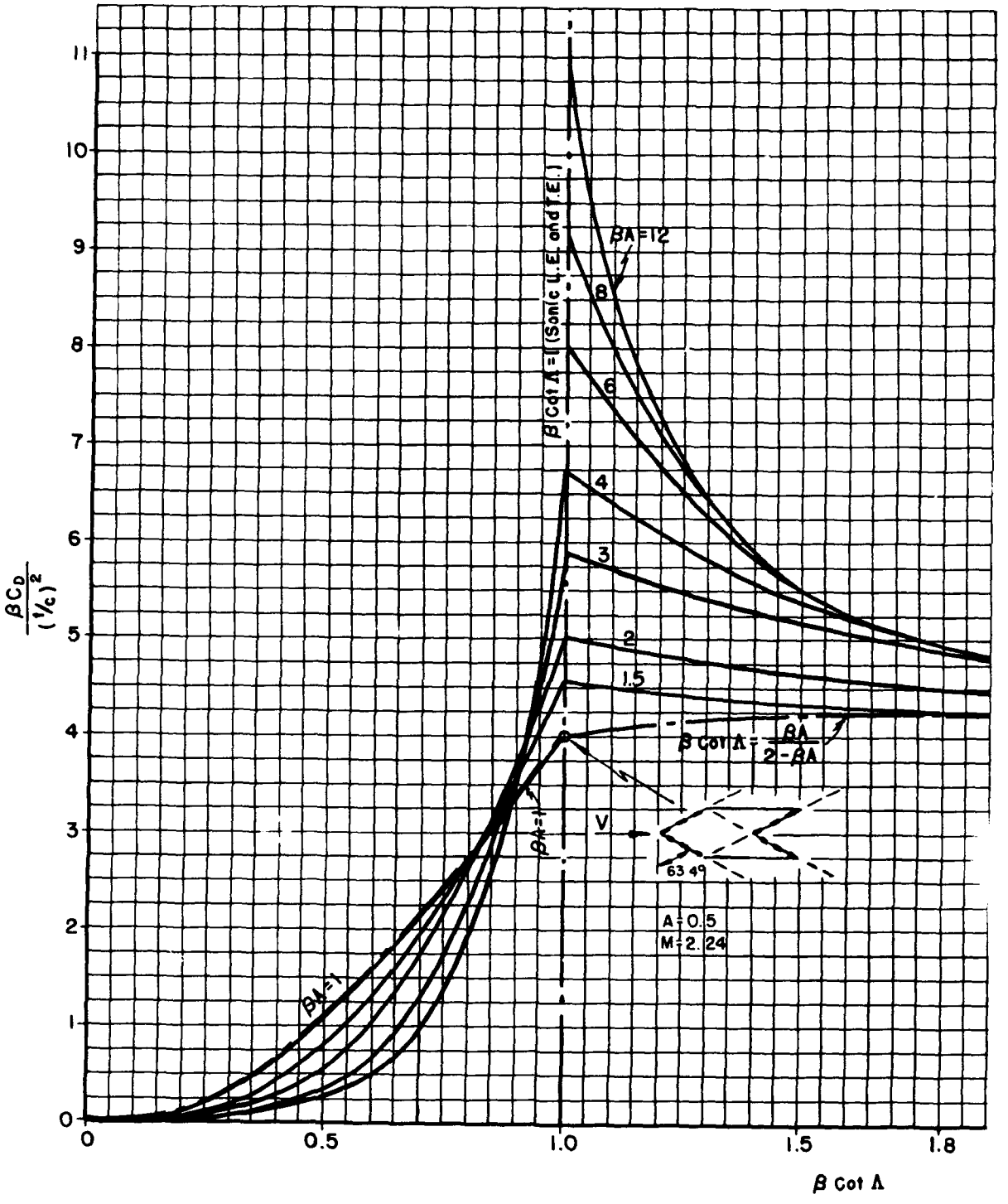

702.23 Figure 12 Generalized curves of the wing pressure-drag parameter at zero lift for untapered wings with

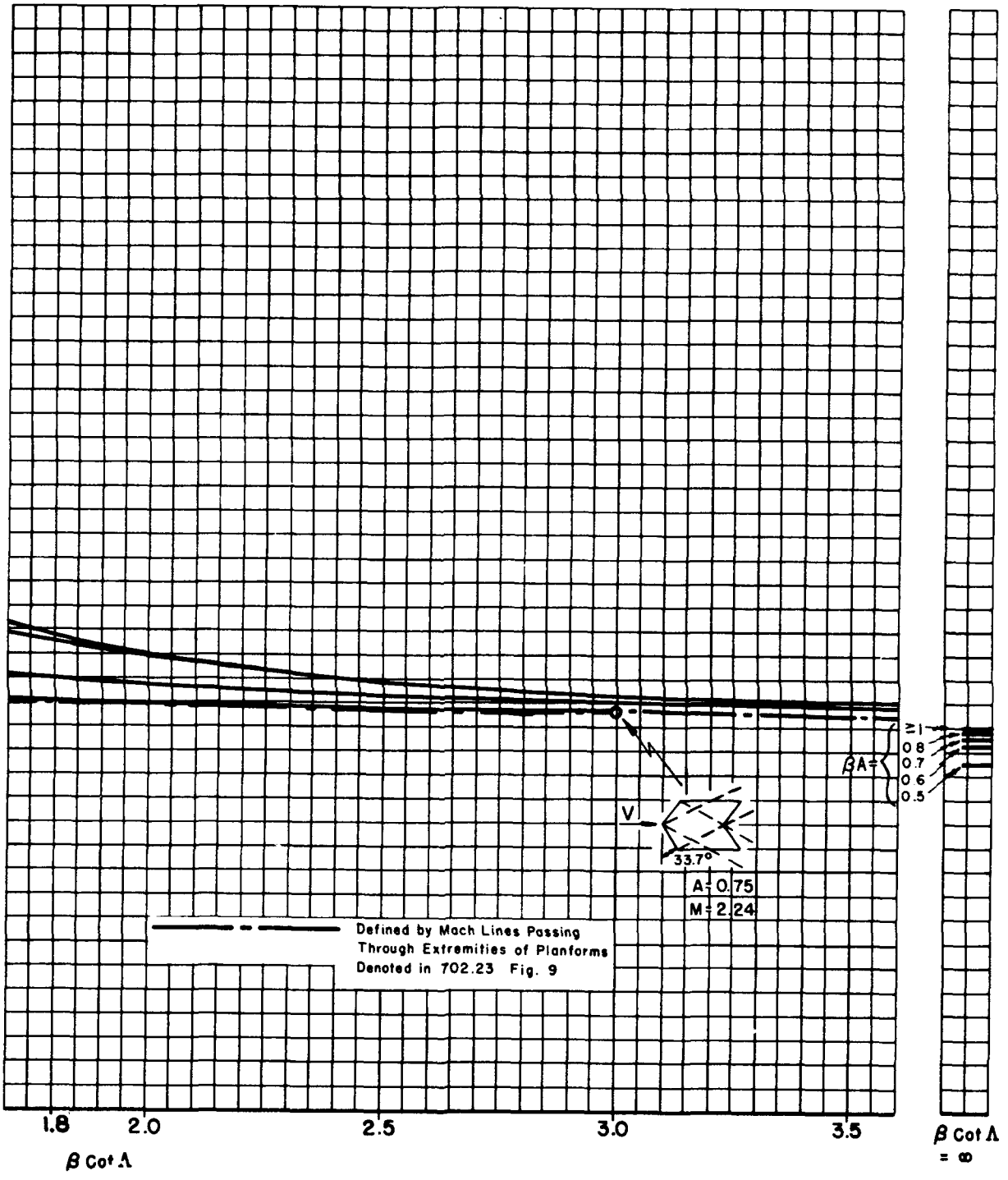

swept leading edges; double wedge profile, maximum thickness at 0.5 chord, λ = 1.0.

489030 O - 59 - 5

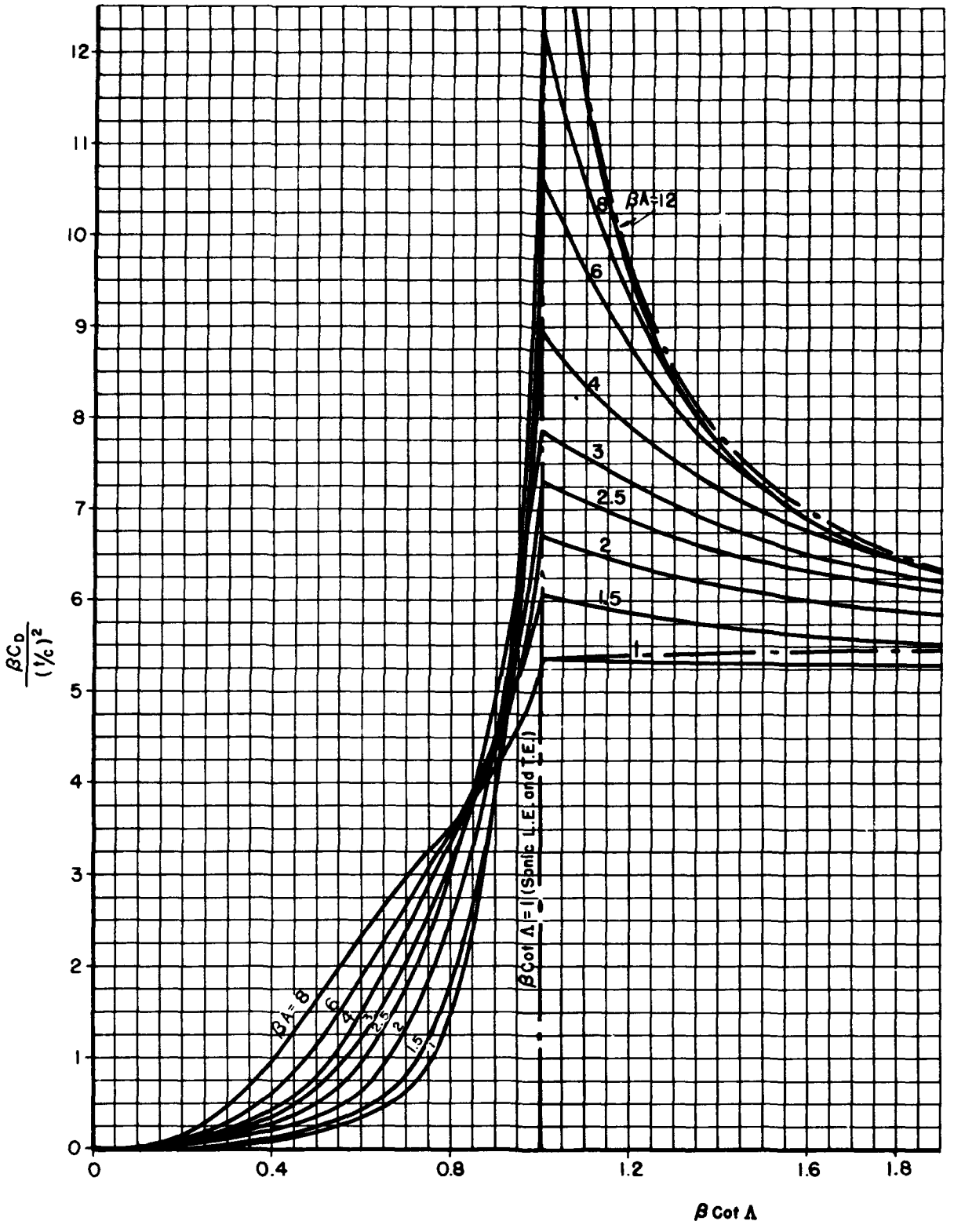

702.23 Figure 13 Generalized curves of the wing pressure-drag parameter at zero lift for untapered wings with

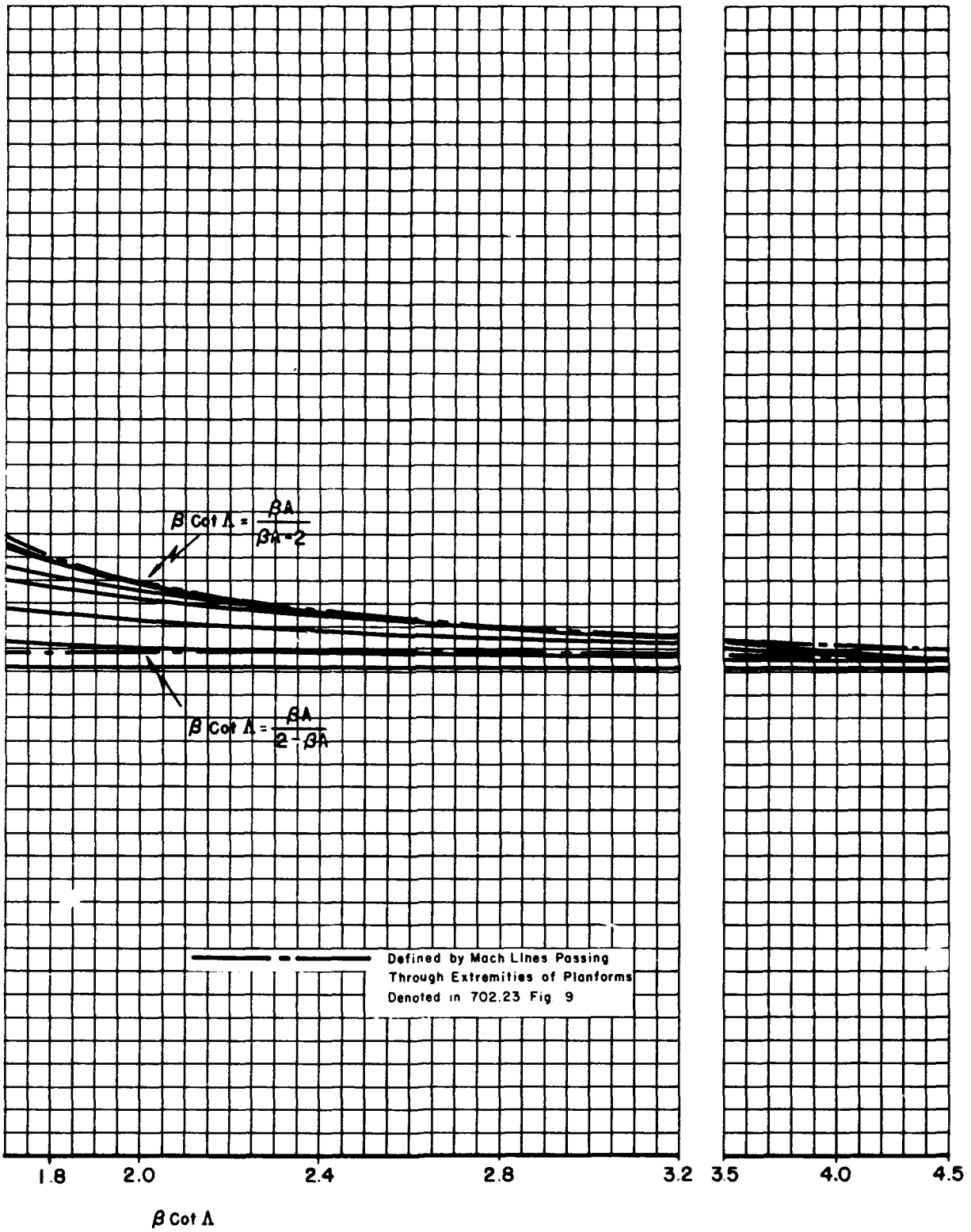

swept leading edges; biconvex parabolic-arc profile, maximum thickness at 0.5 chord, λ = 1.0.

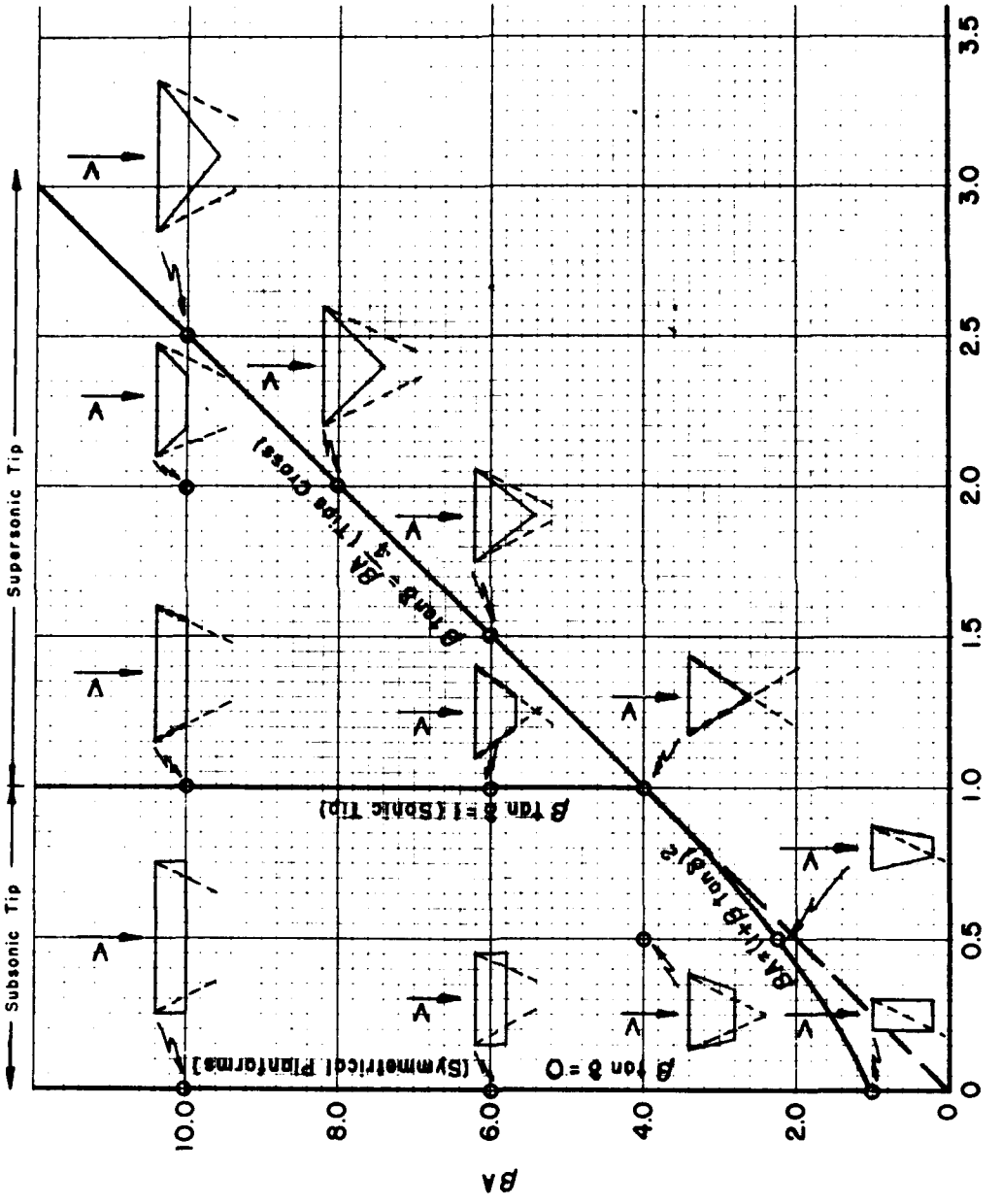

702.11 Fig. 5 Variations in planform associated with changes in parameters βA and $\beta \tan\delta$, Trapezoidal planforms

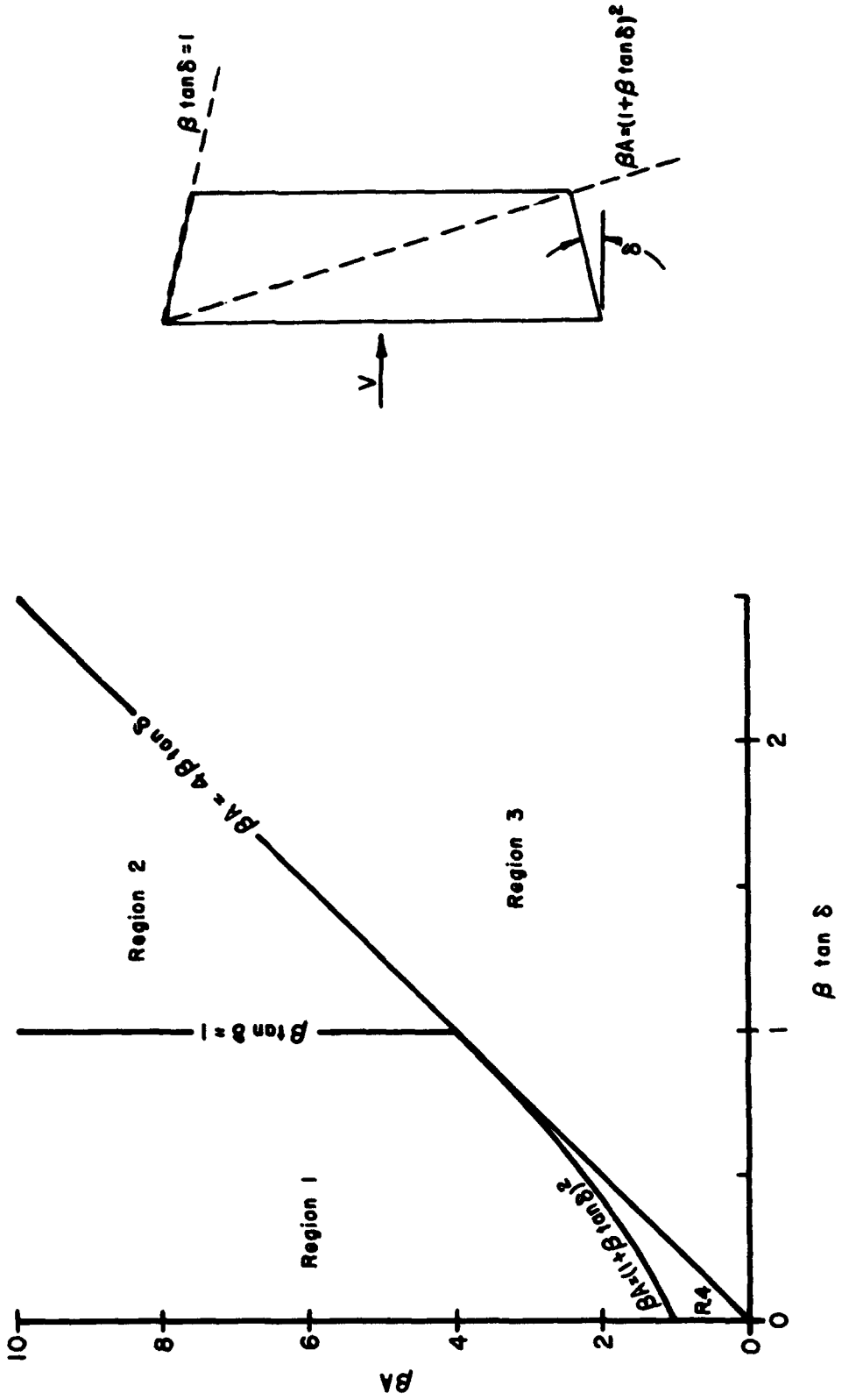

702.23 Figure 14 Composite diagram showing the areas of solution and primary reference sources for the lift, moment, and drag curves, trapezoidal planform.

	Region	Source References
C_{L_α}	1	Replotted from DRL, Eq. 704.26 (Ref. 12). Based on Jones, Appendix C, p. 54 (Ref. 33).
	2	Replotted from DRL, Eq. 704.28 (Ref. 12). Based on Jones, Appendix C, p. 54 (Ref. 33).
	3	No solution obtained.
	4	Solution obtained on tan δ = 0 line (rectangular wing) for $\beta A \geq 1/2$ (Ref. 11). No other solution obtained. Influence of leading edge tip crosses opposite raked tip.
C_{m_α}	1	Replotted from DRL, Eq. 704.27 (Ref. 12). Based on Jones, Appendix C, p. 54 (Ref. 33).
	2	Replotted from DRL, Eq. 704.29 (Ref. 12). Based on Jones, Appendix C, p. 54 (Ref. 33).
	3	No solution obtained.
	4	Solution obtained on tan δ = 0 line (rectangular wing) for $\beta A \geq 1/2$ (Ref. 11). No other solution obtained. Influence of leading edge tip crosses opposite raked tip.
C_D	1, 2, 3	No solution obtained.
	4	Solution obtained only on tan δ = 0 line (rectangular wing) for $\beta A \geq 1/2$ (Ref. 38). Replotted in Fig. 702.23-12, $\beta \cot \Lambda = \infty$. No other solutions obtained.

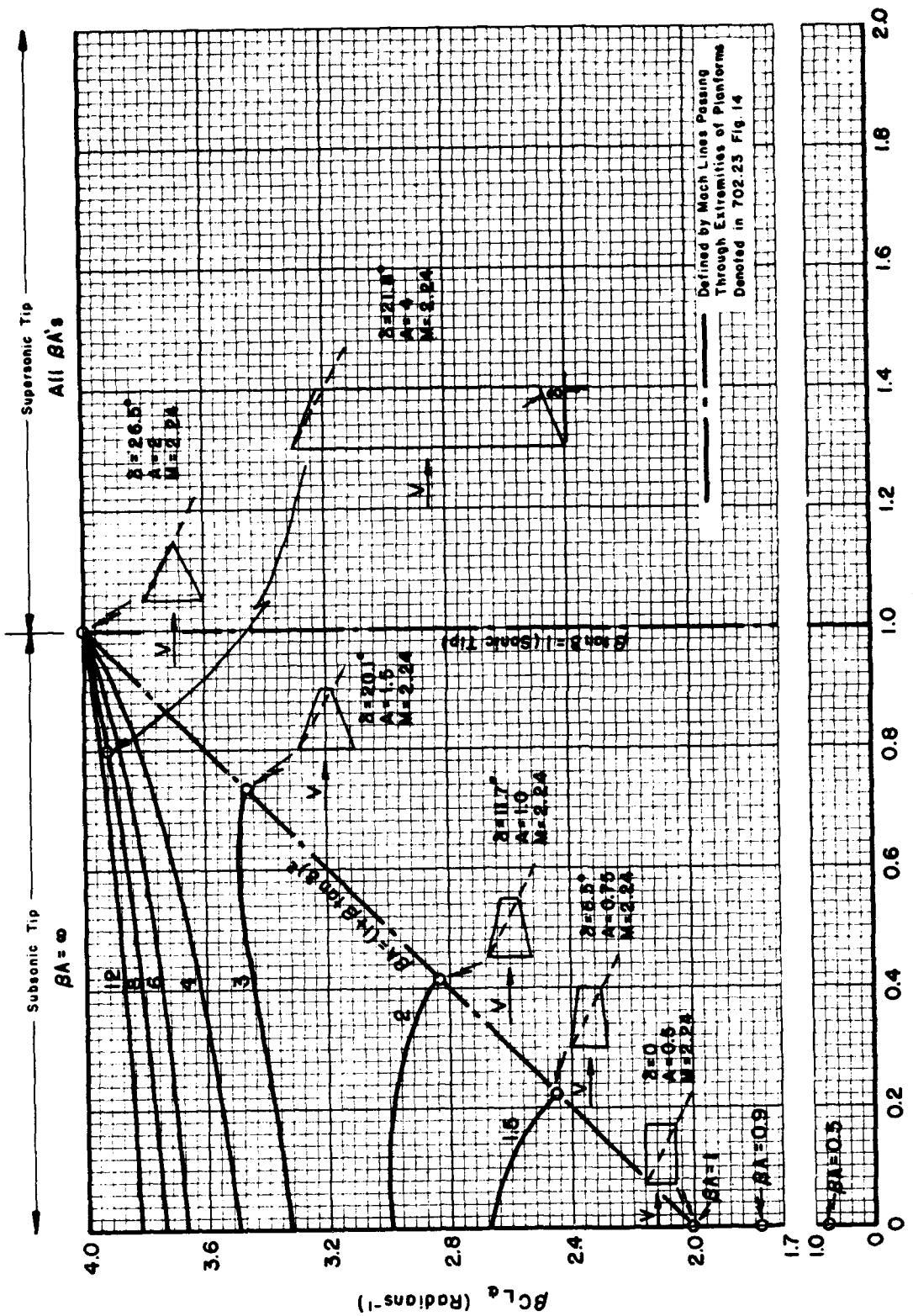

702.23 Figure 15 Generalized curves of the wing lift-curve-slope parameter for trapezoidal wings.

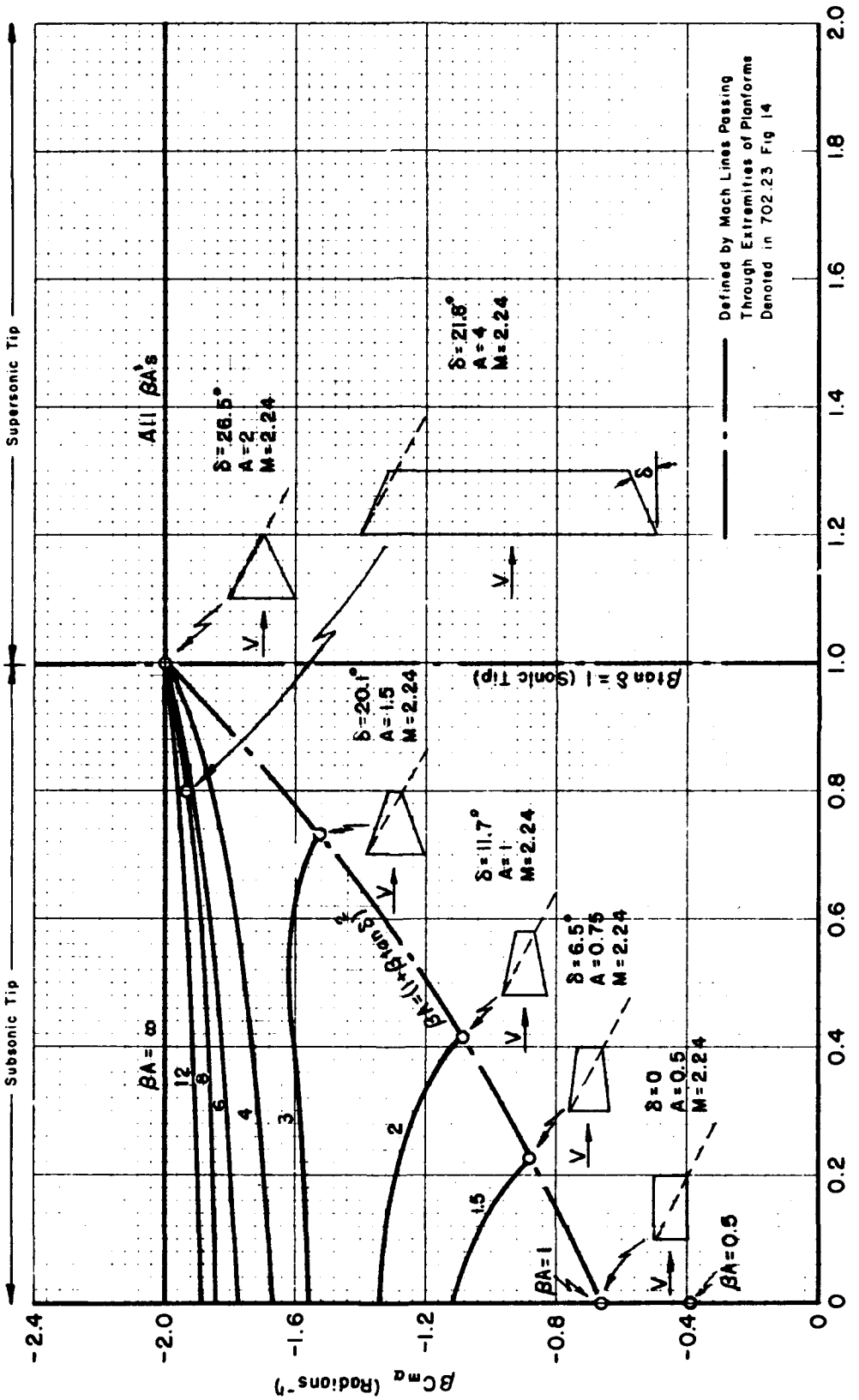

702.23 Figure 16 Generalized curves of the wing moment-curve-slope parameter for trapezoidal wings.

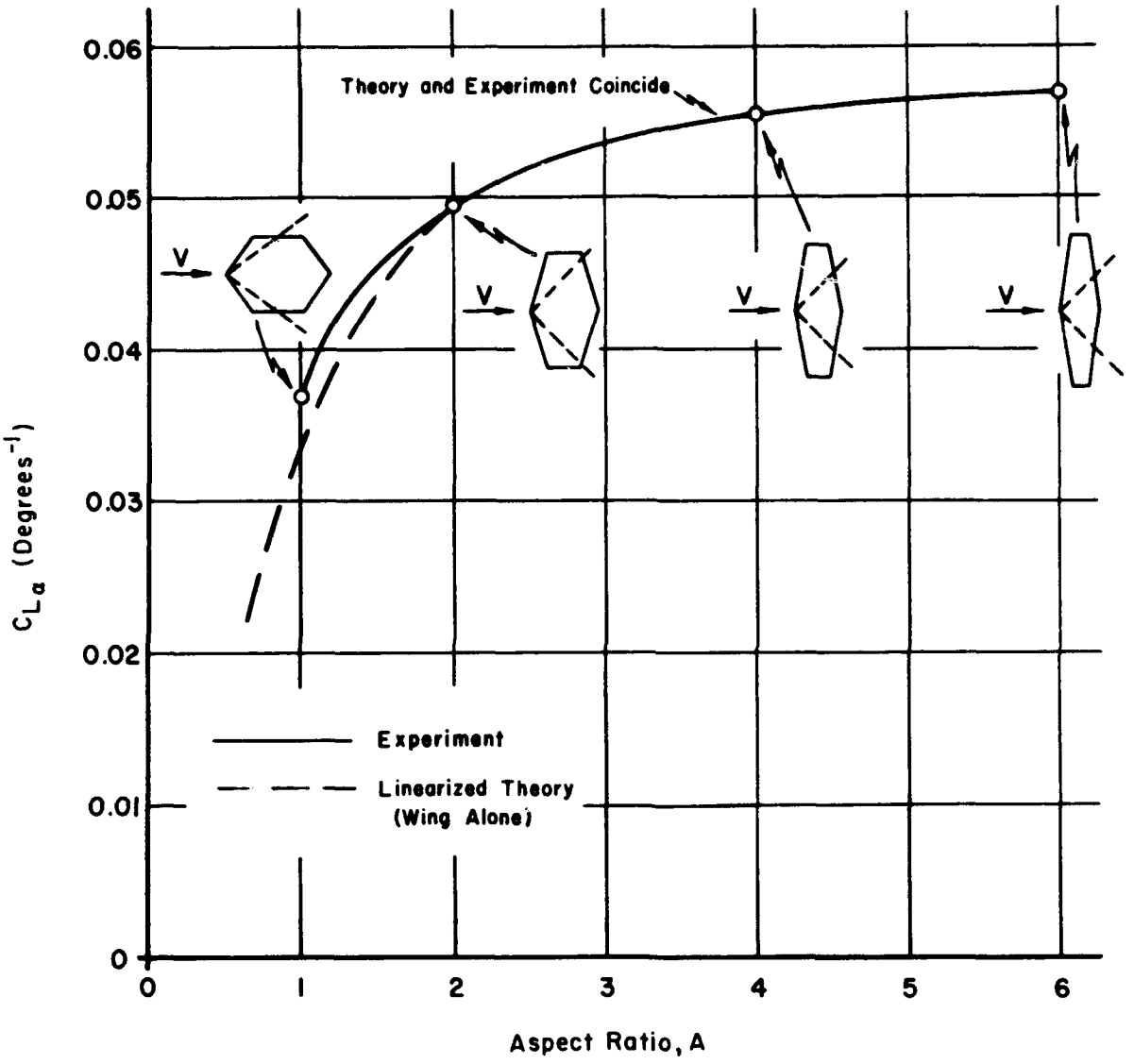

704 Figure 1 Effect of aspect ratio on the lift-curve-slope, $M_\infty = 1.53$, $\lambda = 0.5$, $R_e = 750,000$ (based on the mean geometric chord of the wing). (Ref. 28.)

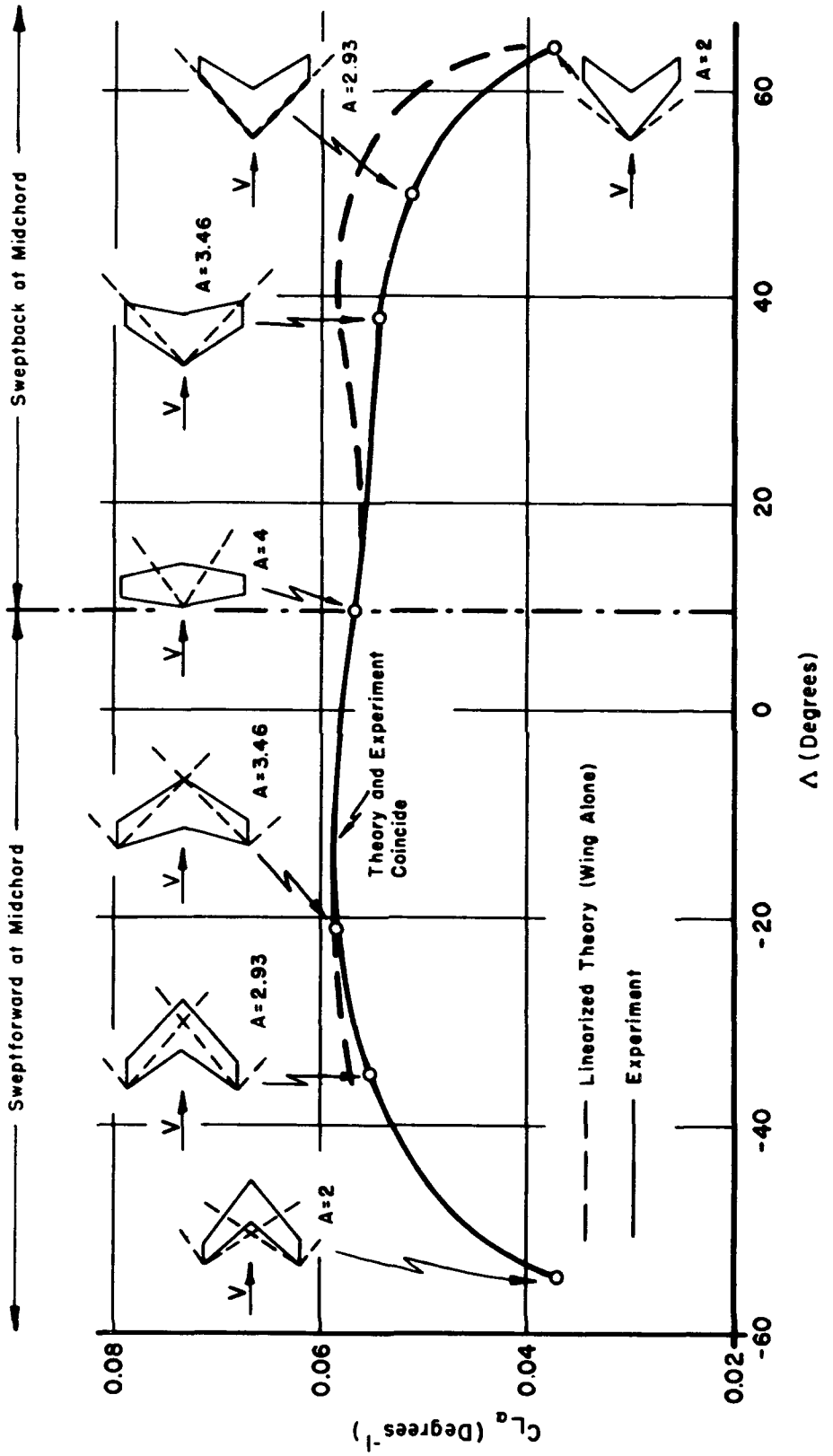

704 Figure 2 Effect of sweep on the lift-curve-slope, $M_\infty = 1.53$, $\lambda = 0.5$, $R_e = 750,000$ (based on the mean geometric chord of the wing). (Ref. 28.)

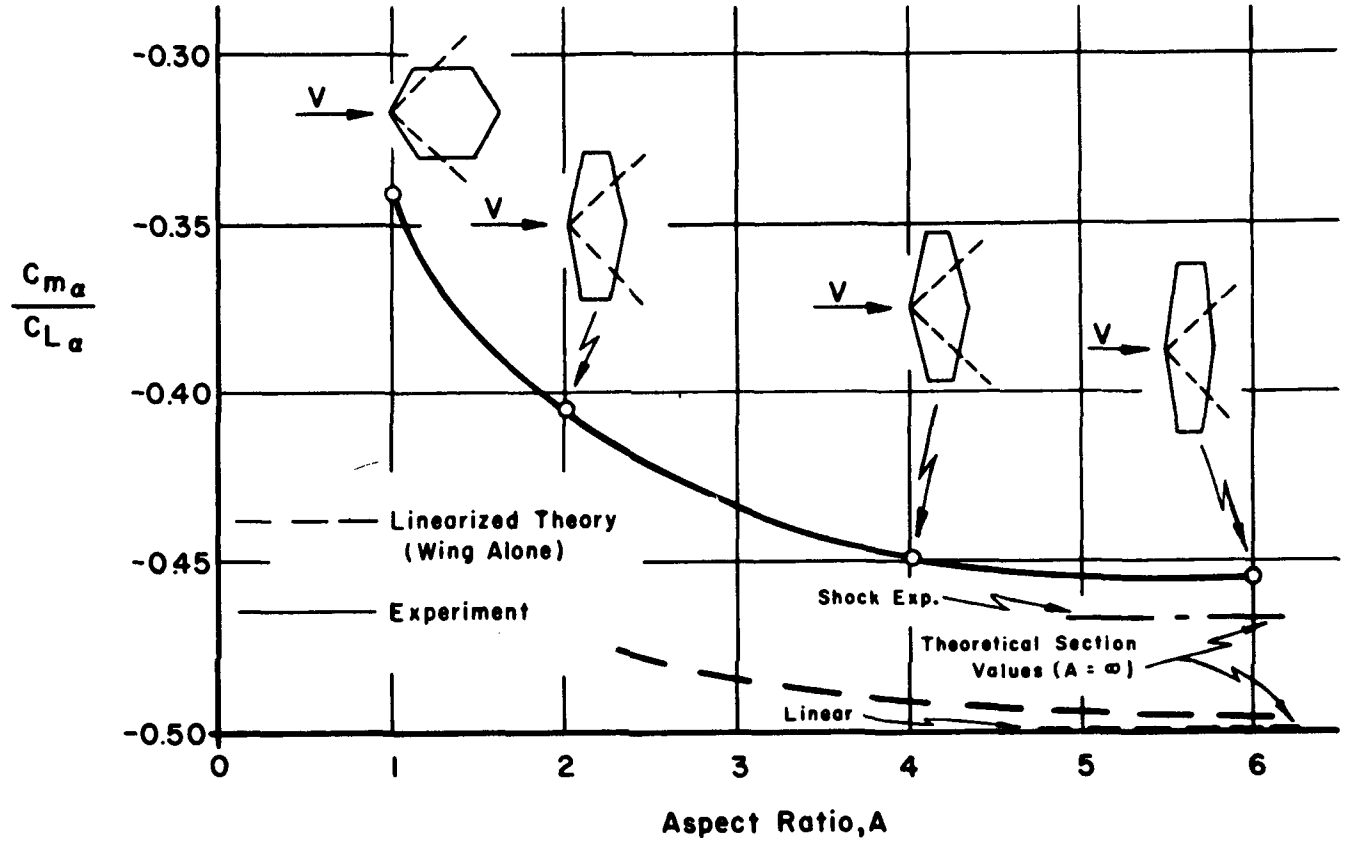

704 Figure 3 Effect of aspect ratio on the center of pressure*, M_∞ = 1.53 λ = 0.5, R_e = 750,000 (based on the mean geometric chord of the wing). (Ref. 28.)

*Center of pressure in fraction of root chord of the wing, aft of the apex of the leading edge and equal to $-C_{m_\alpha}/C_{L_\alpha}$.

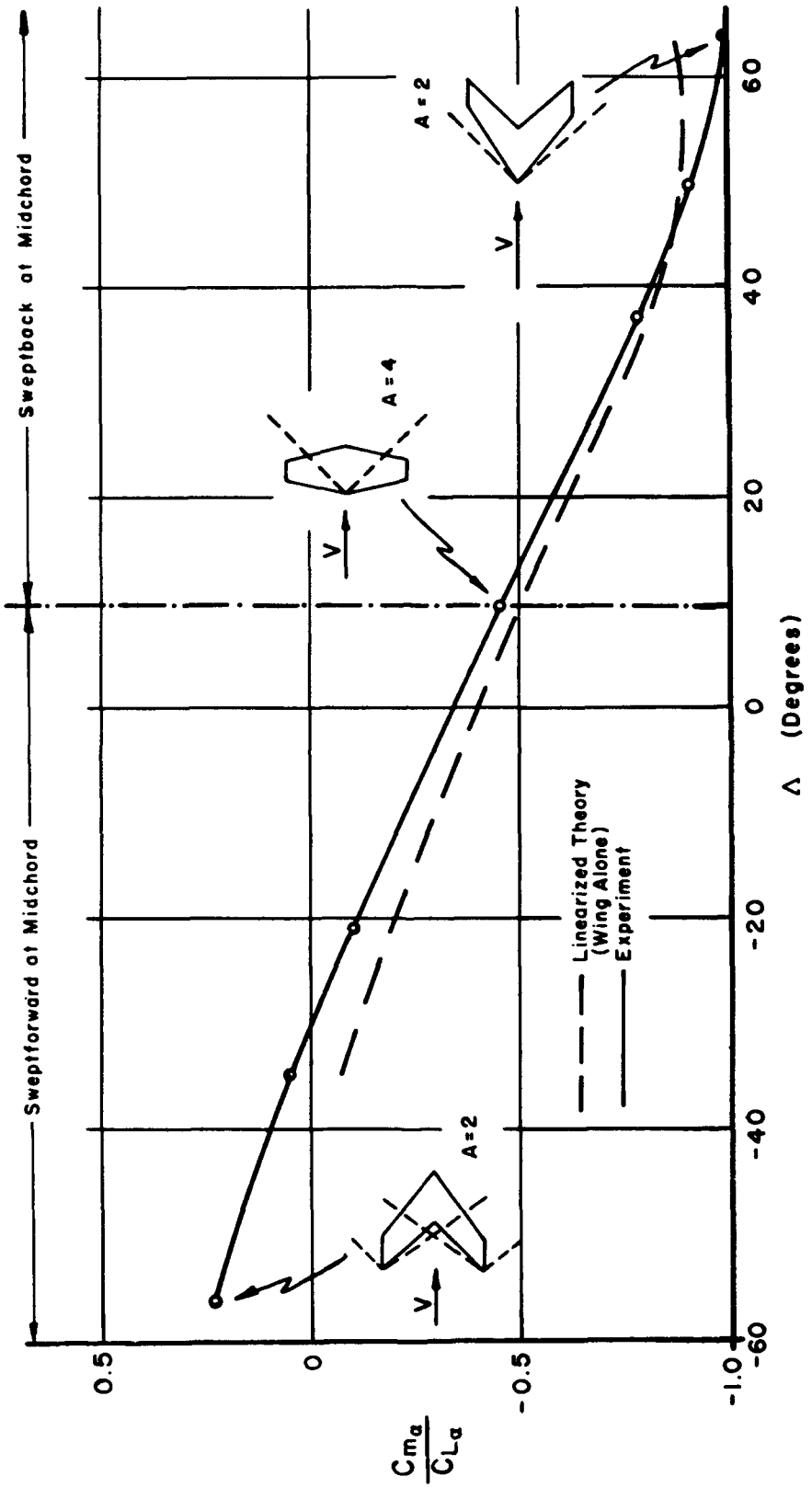

704 Figure 4 Effect of sweep on the center of pressure*, $M_\infty = 1.53$, $\lambda = 0.5$, $R_e = 750,000$ (based on the mean geometric chord of the wing). (Ref. 28.)

*Center of pressure in fraction of root chord of the wing, aft of the apex of the leading edge and equal to $-C_{m_\alpha}/C_{L_\alpha}$.

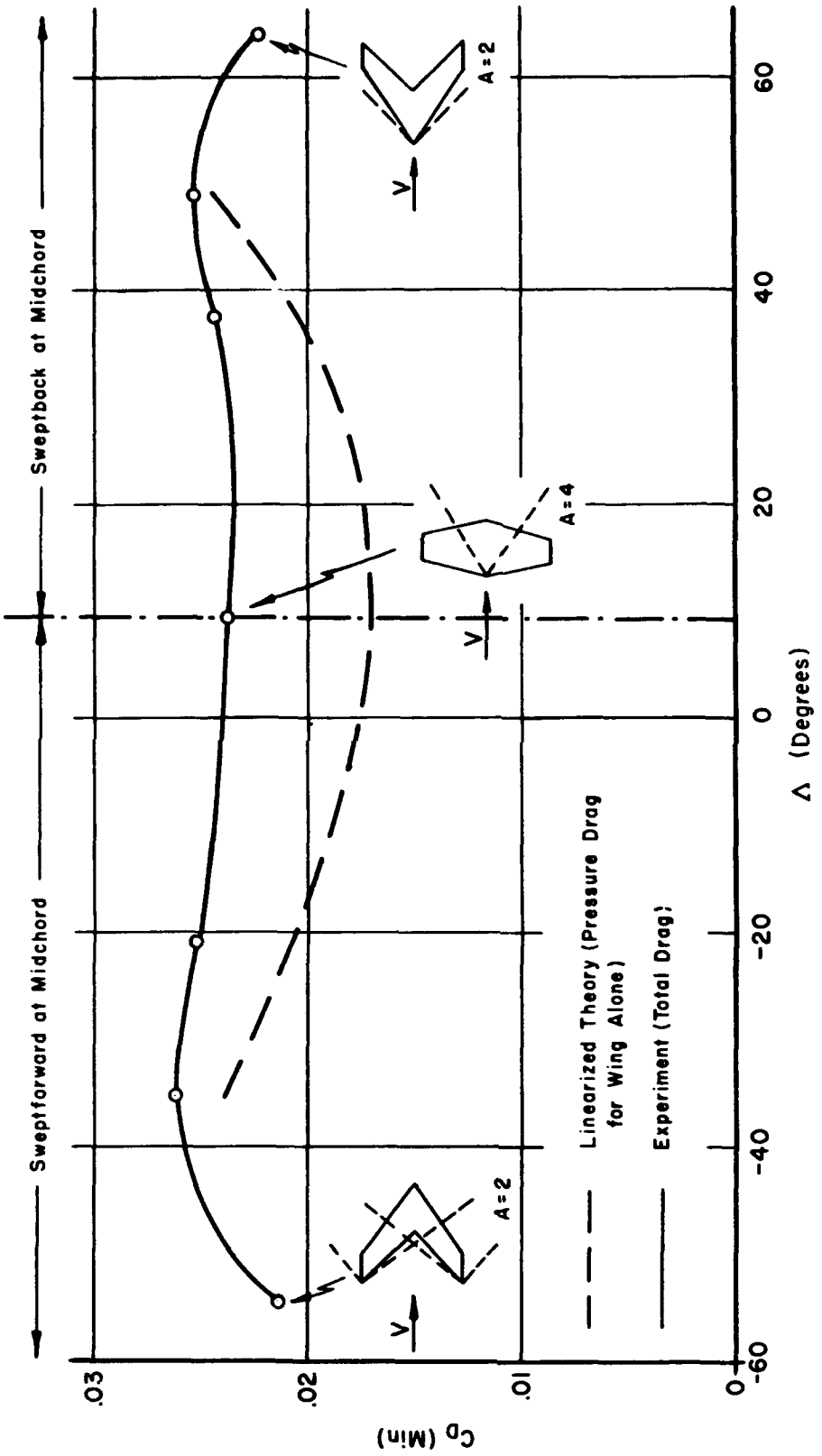

704 Figure 5 Effect of sweep on minimum drag. Results on a 5 per cent thick isosceles triangular cross-section measured at that angle of attack to give a minimum drag. $M_\infty = 1.53$, $\lambda = 0.5$, $R_e = 750,000$ (based on the mean geometric chord of the wing). (Ref. 28.)

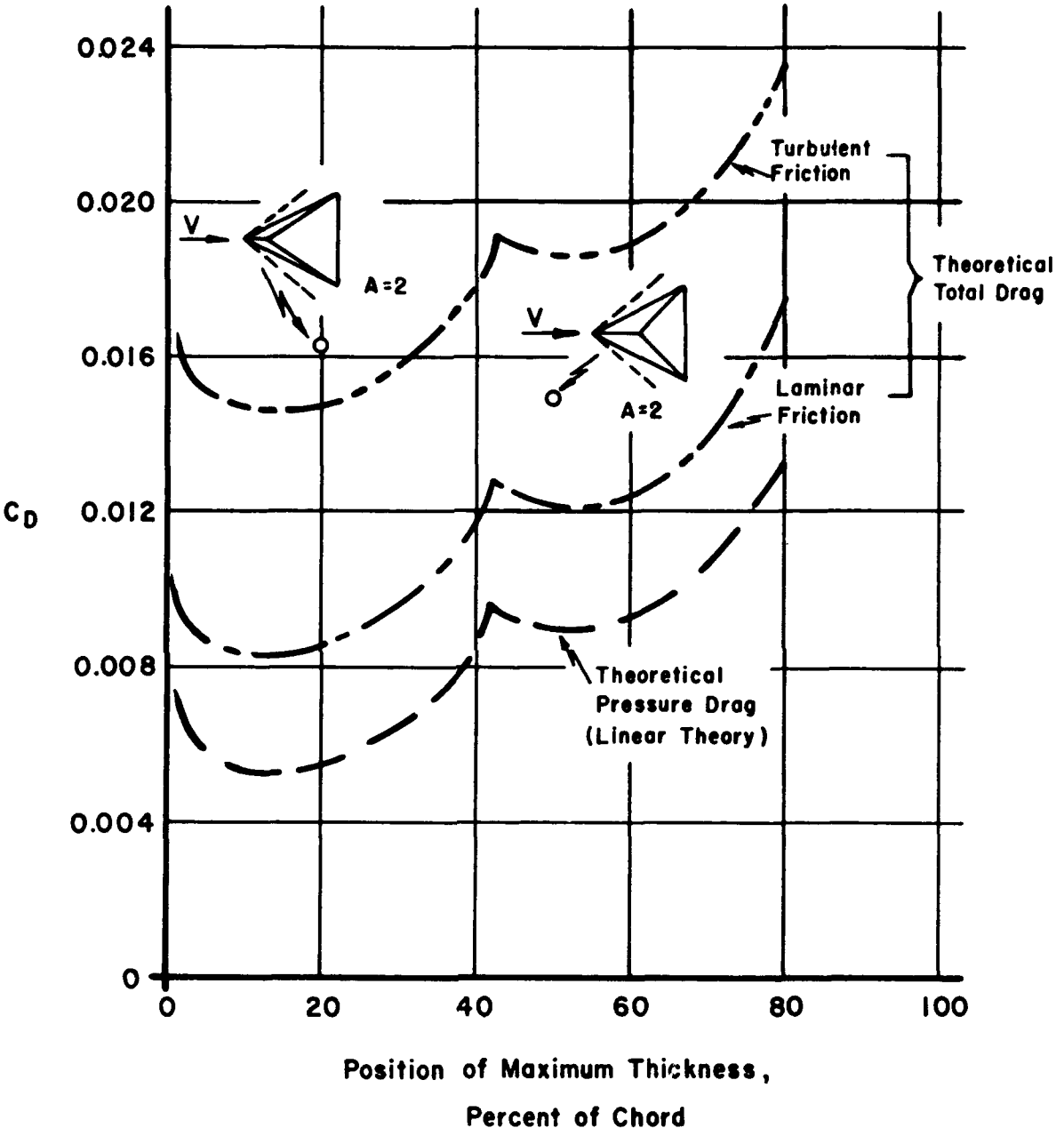

704 Figure 6 Effect of position of maximum thickness on the minimum drag of an uncambered triangular wing; double wedge profile, $M_\infty = 1.53$, $\frac{t}{c} = 0.05$, $\lambda = 0$, $\alpha = 0$, and $R_e = 750,000$ (based on the mean geometric chord of the wing). (Ref. 28.)

SECTION 7 - THREE-DIMENSIONAL AIRFOILS

REFERENCES

1 Applied Physics Laboratory, The Johns Hopkins University. Handbook of Supersonic Aerodynamics. NAVORD Report 1488, Vol. 1. Washington: U. S. Government Printing Office, 1 April 1950.

2 Puckett, Allen E. "Supersonic Wave Drag of Thin Airfoils," J. Aeronaut. Sci., Vol. 13 (September 1946), pp. 475-484.

3 Heaslet, Max A. and Lomax, Harvard. "Three-Dimensional Supersonic Steady State Flow." High Speed Aerodynamics and Jet Propulsion, Vol. VI, Sec. D (edited by W. R. Sears). Princeton: Princeton University Press, 1954, p. 149.

4 Glauert, H. "The Effect of Compressibility on the Lift of Airfoils," Proc. Roy. Soc. (London), Vol. 118 (1927), p. 113.

5 Stewart, H. J. "The Lift of a Delta Wing at Supersonic Speeds," Quart. Appl. Math., Vol. IV (October 1946), pp. 246-254.

6 Busemann, Adolf. Infinitesimal Conical Supersonic Flow. NACA TM 1100, 1947.

7 Evvard, John C. Use of Source Distributions for Evaluating Theoretical Aerodynamics of Thin Finite Wings at Supersonic Speeds. NACA Report 951, 1950.

8 Lagerstrom, P. A. Linearized Supersonic Theory of Conical Wings. NACA TN 1685, 1950.

9 Mirels, Harold. Lift-Cancellation Technique in Linearized Supersonic-Wing Theory. NACA TN 2145, August 1950.

10 Cohen, Doris. Formulas for the Supersonic Loading, Lift, and Drag of Flat Swept-Back Wings with Leading Edges Behind the Mach Lines. NACA Report 1050, 1951.

11 Piland, Robert O. Summary of the Theoretical Lift, Damping-In-Roll, and Center-Of-Pressure Characteristics of Various Wing Plan Forms at Supersonic Speeds. NACA TN 1977, 1949.

12 Aeromechanics Division of the Defense Research Laboratory. Theoretical Lift, Drag, and Pitching Moment Characteristics of Finite Wings of Various Plan Forms at Supersonic Speeds. DRL Report 314. Austin, Texas: The Defense Research Laboratory, The University of Texas, 21 November 1952.

13 Puckett, Allen E. and Stewart, H. J. "Aerodynamic Performance of Delta Wings at Supersonic Speeds," J. Aeronaut. Sci., Vol. 14 (October 1947) p. 567.

489030 O - 59 - 6

14 Jones, Robert T. Thin Oblique Airfoils at Supersonic Speed. NACA Report 851, 1946.

15 Margolis, Kenneth. Supersonic Wave Drag of Sweptback Tapered Wings at Zero Lift. NACA TN 1448, October 1947.

16 Margolis, Kenneth. Effect of Chordwise Location of Maximum Thickness on the Supersonic Wave Drag of Sweptback Wings. NACA TN 1543, March 1948.

17 Margolis, Kenneth. Supersonic Wave Drag of Nonlifting Sweptback Tapered Wings with Mach Lines Behind the Line of Maximum Thickness. NACA TN 1672, August 1948.

18 Harmon, Sidney M. and Swanson, Margaret D. Calculations of the Supersonic Wave Drag of Nonlifting Wings with Arbitrary Sweepback and Aspect Ratio. NACA TN 1319, May 1947.

19 Harmon, Sidney, M. Theoretical Supersonic Wave Drag of Untapered Sweptback and Rectangular Wings at Zero Lift. NACA TN 1449, October 1947.

20 Chang, Chieh-Chien. Applications of Von Karman's Integral Method in Supersonic Wing Theory. NACA TN 2317, March 1951.

21 Lawrence, T. Charts of the Wave Drag of Wings at Zero Lift. TN Aero. 2139 (Revised). Ministry of Supply, Aeronautical Research Council. London: Her Majesty's Stationery Office, 1952.

22 Munk, M. M. The Reversal Theorem of Linearized Supersonic Airfoil Theory. NOL Memorandum 9624. White Oak, Maryland: Naval Ordnance Laboratory, 26 July 1948.

23 Von Karman, Theodore. "Supersonic Aerodynamics--Principles and Applications," J. Aeronaut. Sci., Vol. 14 (July 1947) pp. 373-409.

24 Hayes, Wallace D. Linearized Supersonic Flow. Report AL-222. Los Angeles: North ican Aviation, Inc., 18 June 1947.

25 Hayes, Wallace D. Rev Flow Theorems in Supersonic Aerodynamics. Report AL- . Los Angeles: North American Aviation, Inc., 20 August 1948.

26 Harmon, Sidney M. Theoretical Relations Between the Stability Derivatives of a Wing in Direct and in Reverse Supersonic Flow. NACA TN 1943, 1949.

27 Brown, Clinton E. The Reversibility Theorem for Thin Airfoils in Subsonic and Supersonic Flow. NACA TN 1944, September 1949.

28 Vincenti, Walter G. Comparison Between Theory and Experiment for Wings at Supersonic Speeds. NACA TN 2100, June 1950.

29 Hilton, W. F. High Speed Aerodynamics. New York: Longmans, Green and Co., 1951.

30 Shapiro, Ascher H. The Dynamics and Thermodynamics of Compressible Fluid Flow. Vols. I and II. New York: The Ronald Press Co., 1953-1954.

31 Van Dyke, Milton D. A Study of Second-Order Supersonic-Flow Theory. NACA TN 2200, January 1951.

32 Cohen, Doris. The Theoretical Lift of Flat Swept-Back Wings at Supersonic Speeds. NACA TN 1555, March 1948.

33 Jones, Arthur L., Sorenson, Robert M., and Lindler, Elizabeth E. The Effects of Sideslip, Aspect Ratio, and Mach Number on the Lift and Pitching Moment of Triangular, Trapezoidal, and Related Plan Forms in Supersonic Flow. NACA TN 1916, August 1949.

34 Lapin, Ellis. Charts for the Computation of Lift and Drag of Finite Wings at Supersonic Speeds. Report SM-13480. Santa Monica, Calif.: Douglas Aircraft Company, 1949.

35 Lighthill, M. J. "Higher Approximations." High Speed Aerodynamics and Jet Propulsion, Vol. VI, Sec. E (edited by W. R. Sears). Princeton: Princeton University Press, 1954, pp. 477-489.

36 Multhopp, H. and Winter, M. Charts for the Calculation of the Wave Drag of Swept Wings. TM Aero. 103 (Reprinted). Farnborough, England: Royal Aircraft Establishment, July 1950.

37 Jones, Robert T. and Cohen, D. "Aerodynamics of Wings at High Speeds." High Speed Aerodynamics and Jet Propulsion, Vol. VII, Sec. A (edited by A. F. Donovan and H. R. Lawrence). Princeton: Princeton University Press, 1957, pp. 156-165.

38 Nielsen, J. N. Effect of Aspect Ratio and Taper on the Pressure Drag at Supersonic Speeds of Unswept Wings at Zero Lift. NACA TN 1487, November 1947.

Subsection Number

B

C

D

E

F

G

H

I

U. S. GOVERNMENT PRINTING OFFICE : 1959 O - 489030